Critical properties and vapor-liquid equilibrium of two near-azeotropic mixtures containing HFOs

Zhiqiang Yang, Alain Valtz, Christophe Coquelet, Jiangtao Wu, Jian Lu

Critical properties and vapor-liquid equilibrium of two near-azeotropic mixtures containing HFOs

Zhiqiang Yang[a,c], Alain Valtz[b], Christophe Coquelet[b] *, Jiangtao Wu[c], Jian Lu[a]*

[a] State Key Laboratory of Fluorine & Nitrogen Chemicals, Xi'an Modern Chemistry Research Institute, Xi'an, 710065, China

[b] Mines Paristech, PSL University, CTP -Centre of Thermodynamics of Processes, 35 rue Saint-Honoré, 77300 Fontainebleau, France

[c] Key Laboratory of Thermo-Fluid Science and Engineering, Ministry of Education, Xi'an Jiaotong University, Xi'an, 710049, China

* Corresponding author. E-mail address: christophe.coquelet@mines-paristech.fr. Telephone: +33164694962

*Corresponding author. E-mail address: lujian204@gmail.com (J. Lu). Telephone: +86-29-88291213

Graphical Abstract

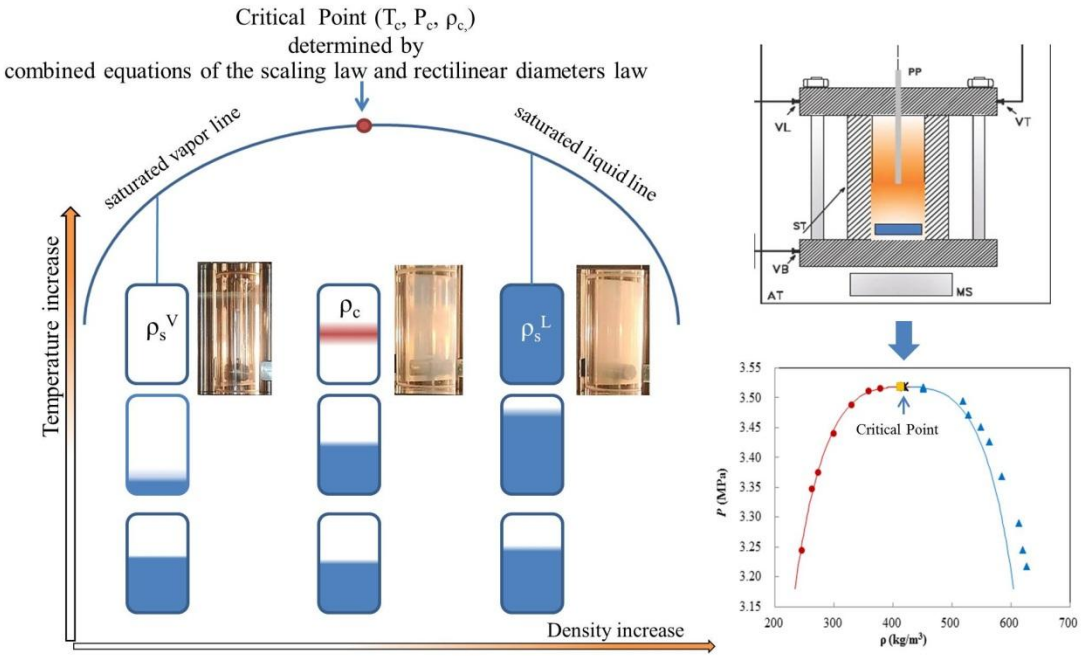

Abstract

This work studies two binary mixtures of R1243zf + R1234yf and R1243zf + R245cb which can be possibly used as a long-term alternative refrigerant for heat pumps. We present critical property (critical temperature, pressure, density) and vapor liquid equilibrium (VLE) of R1243zf + R1234yf and R1243zf + R245cb two binaries. The maximum extended uncertainties (k=2) are estimated as U(T) = 0.21 K, U(p) = 0.048 MPa, and U(ρ) = 6.4 kg/m^3 for critical property measurement, and U(T) = 0.06 K and U(p) = 0.015 MPa for bubble point measurement. The uncertainty of liquid-phase mole fraction is estimated less than 1.8×10^{-4}. The critical property is investigated by a novel method that determines the critical point via modeling vapor-liquid coexistence points to the combined equations of the scaling law and rectilinear diameters law. The VLE of R1243zf + R1234yf and R1243zf + R245cb binary mixtures in the range of 293.45 to 353.55 K are studied by the static-synthetic method which determines the bubble point via the variable volume cell technique. The experimental bubble points are correlated by the Peng-Robinson (PR) equation of state (EoS) with vdW and MHV2 mixing rules. The modeling results are in good agreement with the measured data. The high temperature VLE of the two binary systems is predicted up to the critical point line by PR-MC-MHV2 model with the optimal binary parameters.

Keywords: Refrigerant blend, low-GWP alternatives, vapor-liquid equilibrium, critical properties, modeling

Nomenclature

	Abbreviation		
GWP	global warming potential	VLE	vapor-liquid equilibrium
GHG	greenhouse gas	ODP	ozone-depleting potential
HFOs	hydrofluoroolefins	vdW	van der Waals mixing rules
HFCs	hydrofluorocarbons	HCFCs	hydrochlorofluorocarbons
PR EoS	Peng-Robinson equation of state	MHV2	modified Huron-Vidal second-order mixing rules
MC	Mathias-Copeman alpha function	NRTL	non-random two-liquid activity model
MRDP	average relative deviation of pressure	*MADy*	average absolute deviation of vapor-composition
BIAS	mean bias	R1234ze(E)	trans-1,3,3,3-Tetrafluoroprop-1-ene
R1243zf	3,3,3-Trifluoropropene	R1234yf	2,3,3,3-Tetrafluoroprop-1-ene
OF	objective function	EoS	equation of state
	Roman		
a	energy parameter of the equation of state	b	covolume parameter of the equation of state
$G_m^{\ E}$	excess Gibbs energy	q	coefficient of MHV2 mixing rule
N	number of data points	p	pressure (Pa)
R	molar gas constant (8.314472 $J.mol^{-1}.K^{-1}$)	T	temperature (K)
u	Combined uncertainty	U	expanded uncertainty
x	liquid phase mole fraction	y	vapor phase mole fraction
n	amount of substance	$m_{1,2,\ 3}$	adjustable parameters
k_{ij}	binary interaction parameter		
	Greek		
α	Temperature dependent alpha function	τ	dimensionless interaction parameters
δ	relative deviation	Δ	absolute deviation
Δg_{ij}	interaction energy parameters of NRTL equation	ω	acentric factor
α_{12}	Relative volatility	ρ	density
	Subscripts		
i, j	molecular species	c	critical property
exp	experimental	cal	calculated
m	mixture	r	reduce temperature

1. Introduction

Climate change is one of the biggest challenges facing all humanity. The main driver of climate change is the greenhouse effect caused by a huge amount of greenhouse gas emissions. The dominate refrigerants are mainly hydrofluorocarbons (HFCs) and hydrochlorofluorocarbons (HCFCs), which exhibit high global warming potential (GWP). The direct emissions of these refrigerants account for about 3% of the total global greenhouse gas emissions (Mclinden et al., 2020). In order to protect the global environment, the international community has signed a series of international conventions such as Montreal Protocol, the Paris Agreement, F-Gas Regulations (European Parliament and The Council of the European Union, 2006), Kigali Agreement (UNEP, 2016), etc., to restrict high GWP refrigerants on a global scale. Reducing greenhouse gas emissions and exploring environmentally friendly refrigerants with low greenhouse effect have become urgent issues facing the refrigeration industry.

3,3,3-trifluoropropene (R1243zf) is one of attractive alternative refrigerants which has been recently proposed to replace R134a in air-conditioning and other applications (Lai, 2014). R1243zf has zero ODP, and a remarkably low GWP of 0.29 compared to R134a of 1430 (González et al., 2015). Furthermore, R1243zf exhibits similar thermodynamic behavior as R134a. The thermodynamic properties (Akasaka, 2016; Brown et al., 2013; Di Nicola et al., 2013; Higashi and Sakoda, 2018) and cycle performance (Brown et al., 2014; Lai, 2014) of R1243zf have been extensively studied. The selection of refrigerant requires comprehensive consideration of environmental, thermodynamic properties, refrigeration performance, safety, economy and other factors (Bobbo et al., 2018). Whereas, taking these factors into consideration, ideal pure refrigerants are almost non-existent because of each pure substance has different degrees of defects (McLinden et al., 2017). The defects of R1243zf is flammable, it's assigned as A2L from the ASHRAE classification. The solution to expand the application range of R1243zf is to develop mixed refrigerants, because the components in mixed refrigerants can complement each other. The mixed refrigerant technology provides a way for applications where pure refrigerant cannot meet. For instance, adding HFC compounds to R1234yf such as R-134a, could improve the cooling capacities in one hand and inhibits the flammability on the other (Raabe, 2013).

High-temperature heat pumps are one of the effective ways to utilize waste heat, which can reduce energy consumption and carbon dioxide emissions accordingly. The design of subcritical cycle heat pumps depends closely on thermodynamics properties, especially vapor-liquid equilibrium (VLE) and critical properties of mixture, when mixtures are involved in thermodynamics cycle. This work is one of our series of studies (Jia et al., 2020; Kou et al., 2019; Yang et al., 2021, 2020, 2019) which aim to develop long-term alternative refrigerants. In this work, a novel method (patent of Mines ParisTech - Armines) for determining critical point of pure compound or mixture is presented and tested. The critical temperatures, pressures, and densities of R1243zf + R1234yf and R1243zf + R245cb two binary systems are investigated based on the novel method. The critical point is determined via modeling vapor-liquid coexistence points to the combined equations of the asymptotic law and rectilinear diameters law. The VLE of the two binary systems in the range of 293.45 to 353.55 K are studied based on static-synthetic method which determines the bubble point via the variable volume cell technique (Coquelet et al., 2019). The bubble points are correlated by the Peng-Robinson (PR) equation of state (EoS) associated with Mathias-Copeman (MC) alpha function, and combined with van der Waals (vdW) and modified Huron-Vidal second-order (MHV2) mixing rules (Dahl and Michelsen, 1990).

2. Experimental

2.1 Materials

The information of samples is summarized in Table 1. The purities of samples are verified by gas chromatographic analysis. All the samples are used without further purification (only degassing). The information of gas chromatography method is described in the *Supplementary Information* and gas chromatograph conditions are given in Table S1.

Table 1. Chemical information.

Compound	Chemical Name	CAS number	Supplier	Purity[a] (Mass%)
3,3,3- trifluoropropene	R1243zf	677-21-4	Synquestlabs	99 %
2,3,3,3-tetrafluoropropene	R1234yf	754-12-1	Climalife	99.5%
1,1,1,2,2-pentafluropropane	R245cb	1814-88-6	Synquest	99 %

[a] Gas Chromatograph analysis

2.2 Measurement of critical properties

The apparatus of critical properties designed based on static-synthetic method was built by CTP at Mines ParisTech (patent of Mines ParisTech - Armines). The apparatus is used to measure the vapor-liquid coexistence point (temperature, pressure, and saturated density in critical region) by visually observing the critical opalescence and the disappearance or reappearance of vapor-liquid interface. The experimental apparatus consists of loading and measurement parts, as shown in Fig. 1, and it's similar to that of Soo et al. (2010), Juntarachat et al. (2012), and Gil et al. (2008).

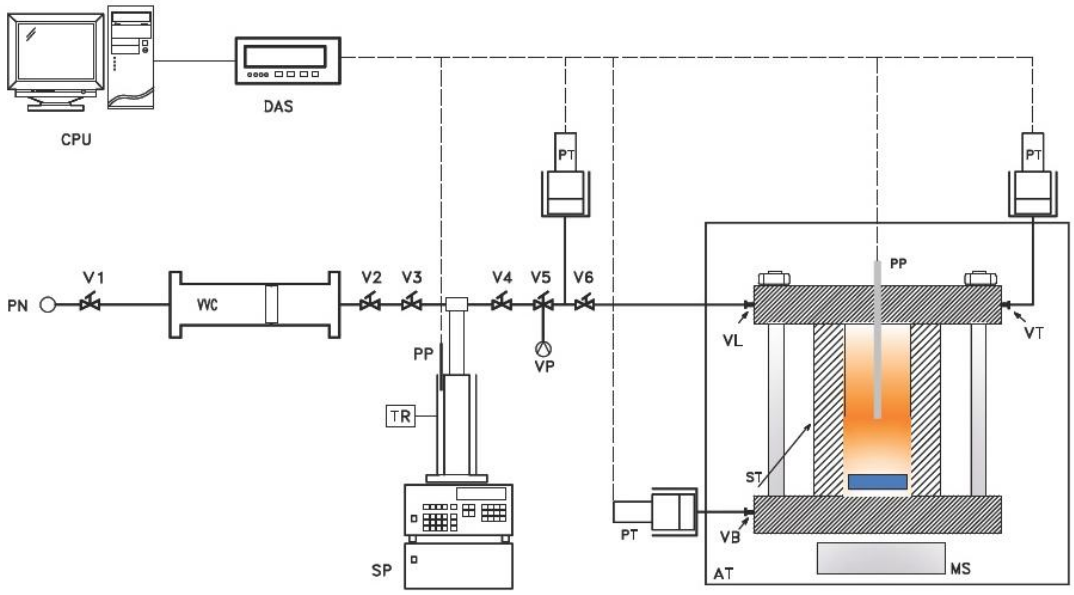

Figure 1. Schematic diagram of the critical properties measurement apparatus.
PS: pressurized source; VVC: variable volumetric cell; SP: syringe pump; VP: vacuum pump; EM: electric motor; MS: magnetic stirrer; ST: sapphire tube; VC: visual cell; AT: air thermostat oven; TP: platinum resistance temperature probe; PT: pressure transducer; TR: temperature regulator; DAS: data acquisition system; CPU: central processor unit; V: valve.

The loading part is very similar to the work described by Soo et al. (2010). It includes a thermostatic syringe pumps (ISCO, model 260D), a variable volumetric cell, and pressure resource (compressed nitrogen). The variable volumetric cell is specially designed to prepare the mixture, and the syringe pump is used to store the synthesized mixture and deliver them to the optical cell. The body of syringe pump is surrounded with an external jacket within which tap water thermally regulates and maintains the pump contents at room temperature. The syringe pump has two control modes: constant flow rate and constant pressure. The latter

mode is utilized to load components into the optical cell.

The core unit of the measuring part is the optical cell which is self-developed by CTP and consists of top flange, bottom flange, and sapphire tube. The sapphire tube and two flanges are sealed with golden O ring. The operating temperature and pressure limits of the optical cell are up to 493 K and 20 MPa. The inner volume of the optical cell is calibrated by filling it with ethanol at room temperature, and the calibration value was 12.915 ± 0.014 cm3. The optical cell is installed in a visual air thermostatic oven (AT) with temperature fluctuation less than 0.1 K. In order to enhance the visibility of the vapor-liquid interface and critical opalescence, a light source is installed in the air thermostatic oven. The volume variation of the optical cell caused by temperature and pressure is negligible, and detailed information for the volume variation can be found in the Appendix SC of *Supplementary Information* .

The temperature in the optical cell is measured by using a 100 Ohm platinum resistance thermometer probe which extends down along the central axis of the sapphire tube from the top flange. Another two platinum probes are inserted into the top flange and the bottom flange, respectively, to monitor the temperature gradient between the top and bottom of the optical cell. The pressure of the optical cell is measured by using two pressure transducers (DRUCK, Model PTX611), one connected to the top flange, the other connected to the bottom flange. The two pressure transducers are maintained at a constant temperature of 373 K using a heating cartridge regulated by a PID regulator (WEST, Model 6100). Another pressure transducer (DRUCK, Model PTX611) is used for measuring the pressure of loading line. The signals from the temperature probes and pressure transducers are recorded by a computer linked to a data acquisition unit (Agilent; HP34970A). The temperature probes, pressure sensors, and volume of the critical cell are well calibrated before measurement, and the information of calibration is described in *Supplementary Information*. The uncertainty of temperature, pressure and density measurement is carefully analyzed, and the information of uncertainty analysis can be found in Appendix SA in *Supplementary Information*. The extended uncertainties (k=2) are estimated as U(T) = 0.06 K, U(p) = 0.001 MPa, and U(ρ) = 6.4 kg/m^3 for critical property measurement.

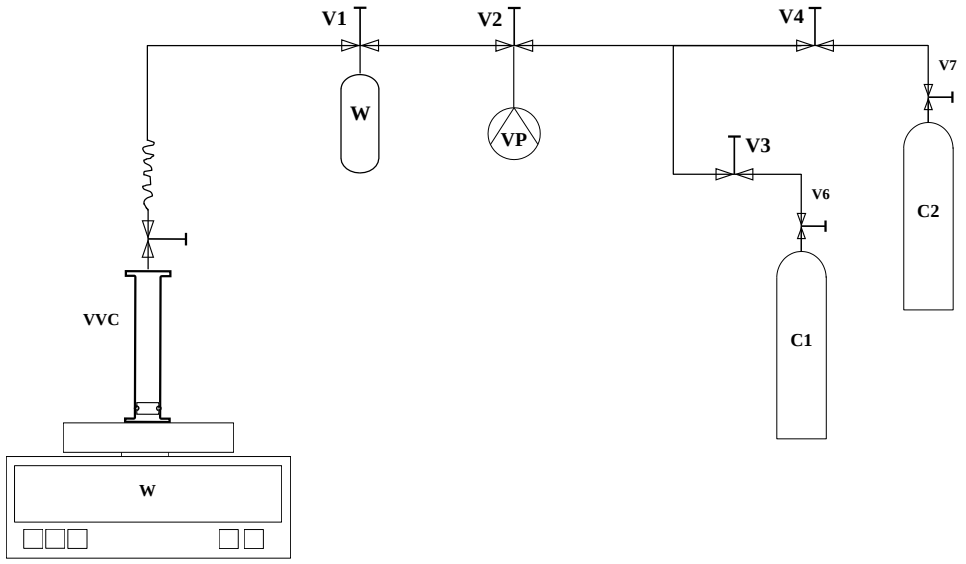

Figure 2. Flow diagram of mixture preparation.
C1: more volatile compound; C2: less volatile compound; V: valve; VVC: variable volumetric cell; W: balance; VP: vacuum pump.

The mixture is prepared in the variable volumetric cell and the concentration of the synthesized mixture can be accurately determined by weighing on a balance (Mettler Toledo, model XP2004S), as illustrated in Figure 2. Then the mixture is compressed and transferred to the syringe pump.

The transfer of sample is carried out in the monophasic liquid state at elevated pressures. Before loading the sample into the optical cell, the sample is compressed again to monophasic liquid and maintained at high pressure for a sufficient amount of time. Such a loading process ensures the composition of the sample remains unchanged. Since the pressure, temperature, and composition of the sample remain unchanged during the loading process, the mass of loaded sample is equal to the compressed density of the sample multiplied by the volume change of the syringe pump. The saturated density (vapor or liquid phase) is calculated by Eq. (1):

$$\rho = \frac{m_{load}}{V_{cell}} = \frac{\rho_T \Delta V}{V_{cell}} \quad (1)$$

Where ρ is saturated density of vapor or liquid; V_{cell} is the volume of the optical cell; m_{load} is the mass of loaded sample; ΔV is the volume change of ISCO pump; ρ_T is the compressed liquid density of sample at loading temperature and pressure. The uncertainty of

saturated density is discussed in Appendix SA of *Supplementary Information*.

For the calculation of saturated density of mixture, Eq. (1) is modified as:

$$\rho_{mix} = \frac{\rho_{mix}\Delta V}{V_{cell}} = \frac{(x_1\rho_1 + x_2\rho_2.)\Delta V}{V_{cell}} \quad (2)$$

where ρ_1 and ρ_2 are the compressed liquid density of components 1 and 2 at loading temperature and pressure; x_1 and x_2 are mole fraction of components 1 and 2.

The mole fraction of each component is determined by Eq. (3)

$$x_1 = \frac{m_1/M_1}{m_1/M_1 + m_2/M_2}\ ; x_2 = 1 - x_1 \quad (3)$$

Where m_1 and m_2 are the mass of components 1 and 2 loaded into the variable volumetric cell, and M_1 and M_2 are their corresponding molar mass. The components mass (m_1 and m_2) are measured by the Mettler Toledo balance, and the accuracy of mass measurement is less than ±0.1 mg. The uncertainty of mole fraction $u(x_1)$ is calculated by following Eq. (4):

$$u(x_1) = x_1(1 - x_1)\sqrt{\sum\left(\frac{u(m_i)}{m_i}\right)^2} \quad (4)$$

Where $u(m_i) = \frac{0.0008}{\sqrt{3}}$ g.

The experimental procedure of critical properties measurement is described in *Supplementary information*. Transition of the measuring sample from subcritical to the critical state on density increase is shown in Figure 3. For each measurement, the temperature-increasing and temperature-decreasing processes are repeated several times.

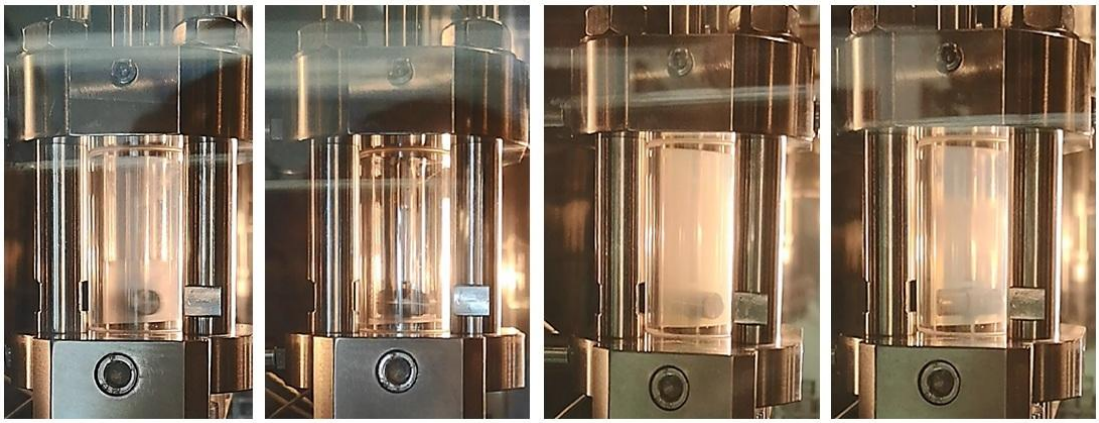

Figure 3. Transition of a fluid from subcritical to the critical state on density increase. From left to right: classical vapor liquid mixture (the two phases are perfectly separated by a thin meniscus); saturated vapor phase (the vapor-liquid interface disappear at the bottom of the optical cell); saturated liquid phase (the vapor-liquid interface disappear at the top of the optical cell. The meniscus becomes thicker and thicker and the liquid phase become cloudy and milky); critical opalescence (vapor-liquid interface disappear at the center level of optical cell, and the meniscus become darkness and occupies the entire optical cell).

2.3 Measurement of vapor liquid equilibrium

The vapor liquid equilibrium (VLE) is measured by a PVT apparatus which has been designed to allow simultaneous determination of bubble pressure through pressure versus volume measurements. The principle of measurement is based on the static-synthetic method which is the same as the previous literature presented by our laboratory (Coquelet et al., 2004; Meskel-Lesavre et al., 1982; Rousseaux et al., 1983; Meekel-leeavre et al., 1981). The version of the apparatus used by Valtz et al. (1986) has been upgraded to version of this work, and the schematic diagram of PVT apparatus is shown in Figure 4. The variable volume cell has been improved to visible sapphire cell. The structure of the sapphire cell is similar to that of critical properties measurement. The sapphire cell contains an automatically controlled piston to perform internal volume changes. When the piston moves from the top towards the bottom, the components in the sapphire cell will be compressed from the state of vapor-liquid coexistence to the state of monophasic liquid. The displacement of the piston can be accurately controlled via an homemade software with the help of servomotor and ball screws. The internal volume is determined by means of a displacement transducer attached to the piston. The sapphire cell is immersed in a visual thermostat bath (NORMALAB, Model ASTM D 445). The temperature in the cell is measured by using two platinum probes which

are inserted into the top flange and the bottom flange, respectively. The pressure in the cell is measured by a miniature pressure transducer (KULITE, Model CPC 8000) which is installed at the bottom of the variable volume cell. The temperature probe and pressure sensors are calibrated before measurement, and the information concerning calibration as well as the experimental procedure of bubble pressure measurement is described in *Supplementary Information*. The uncertainty analysis on temperature and pressure measurements is discussed in Appendix SA of *Supplementary Information*. The extended uncertainties (k=2) are estimated as U(T) = 0.06 K and U(P) = 0.015 MPa for bubble point measurement.

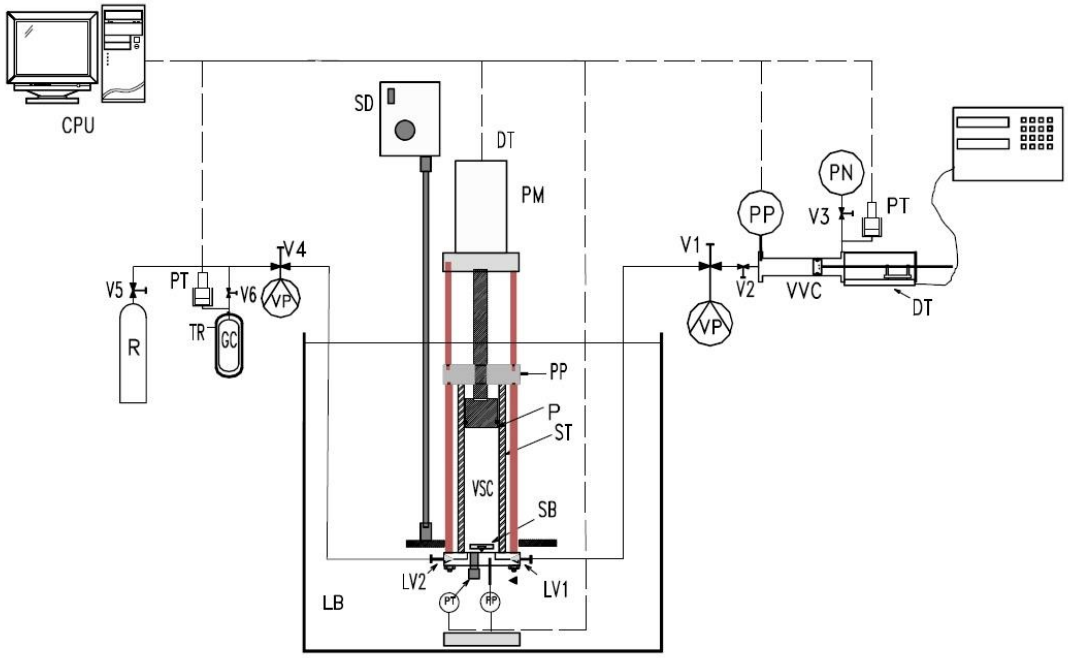

Figure 4. Schematic diagram of the PVT measurement apparatus.

VSC: visual sapphire cell; LV: loading valve; SB: stirrer bar; PM: piston monitor; SD: digital stirrer; P: piston; ST: sapphire tube; VC: visual cell; PP: platinum resistance thermometer probe; PT: pressure transducer; TR: temperature regulator; LB: liquid bath; VVC: variable volume cylinder; DT: displacement detector; GC: gas cylinder; R: refrigerant; V: valve; CPU: central processor unit; VP: vacuum pump.

3 Modeling

3.1 modeling of critical point

For the critical point measurement, whatever dynamic method or static method was utilized, the critical point was normally determined in consideration of the meniscus disappearing level as well as the intensity of critical opalescence, such a criteria can be found

in the open literature (Higashi et al., 2015; Akasaka et al., 2013; Soo et al., 2010; Juntarachat et al., 2012). Different with current visual method, we present a new modeling method that determined the critical point via modeling vapor-liquid coexistence points to the combined equations of the asymptotic law and rectilinear diameters law.

Close to the critical point, fluid exhibit large density fluctuation, and the phase behavior is determined by the size and nature of fluctuation rather than by the particular feathers of the molecular interaction. The phase behavior exhibits universal critical exponents for all fluid in the vicinity of the critical point, which is also called the scaling law or the asymptotic law behavior.

The temperature versus density curve exhibits critical exponent relationship for all pure or mixed systems:

$$\rho^L - \rho^V = B(T - T_c)^\beta \tag{5}$$

Where $\beta = 0.325$ is a characteristic universal exponent, T_c is critical temperature, ρ^L and ρ^V represent saturated density at vapor and liquid phase, and parameter B is a substance dependence constant.

It is also assumed that saturated densities of the coexisting liquid and vapor obey the so-called law of rectilinear diameters:

$$\frac{\rho^L + \rho^V}{2} - \rho_c = A(T - T_c) \tag{6}$$

Combining Eq. (5) with Eq. (6), saturated liquid density ρ^L and saturated vapor density ρ^V can be expressed as:

$$\rho^L = A(T - T_c) + \frac{1}{2}B(T - T_c)^\beta + \rho_c \tag{7}$$

$$\rho^V = A(T - T_c) - \frac{1}{2}B(T - T_c)^\beta + \rho_c \tag{8}$$

These equations were previously used by Coquelet et al. (2010) for the modeling of the volumetric properties of hexafluoropropane at saturation and close to its critical point. Besides, in the critical region, the change of density with pressure obeys following critical exponent principle of the scaling law:

$$\rho = \rho_c(1 \pm C(p - P_c) \pm D(p - P_c)^\beta) \tag{9}$$

Where the +sign refer to density versus pressure curve in the liquid phase, while -sign refer to density versus pressure curve in the vapor phase. Parameters *C* and *D* are substance dependence constant, $\beta = 0.325$ is a characteristic universal exponent.

By separating Eq. (9) into two ranges, ρ^{L} and ρ^{V} can be expressed as following equations:

$$\rho^{L} = \rho_c(1 + C(p - P_c) + D(p - P_c)^{\beta}) \quad (10)$$

$$\rho^{V} = \rho_c(1 - C(p - P_c) - D(p - P_c)^{\beta}) \quad (11)$$

For an investigated pure or mixture system, the vapor-liquid coexistence curve in critical region should satisfy the equations of (7), (8), (10), and (11). The critical temperature T_{c}, critical pressure p_{c}, and critical density ρ_c can be determined based on the knowledge of several liquid-vapor coexistence points. The critical properties T_{c}, p_{c}, ρ_c, and constants *A*, *B*, *C*, and *D* can be regressed by fitting saturated densities to the following objective function Eq. (12).

$$F = \frac{100}{N}\sum_{i}^{N}\left[(\rho_{i,exp}^{V} - \rho_{i,cal}^{V})^2 + (\rho_{i,exp}^{L} - \rho_{i,cal}^{L})^2\right] \quad (12)$$

At least eight data points (four in vapor phase, and four in liquid phase in the vicinity of the critical point) are used for the critical property regression.

3.2 modeling of vapor liquid equilibrium

The experimental bubble pressures were modeling using the Peng-Robinson (Peng and Robinson, 1976) equation of state (PR78 EoS) associating with Mathias-Copeman (MC) alpha function (Mathias and Copeman, 1983). The classical van der Waal one fluid mixing rules and one of excess Gibbs energy (g^E) mixing rules, namely modified Huron-Vidal second-order mixing rules (MHV2) (Dahl and Michelsen, 1990), are employed to describe the VLE behavior of mixture. The NRTL model (Renon and Prausnitz, 1968) is used to calculate g^{E} in the MHV2 mixing rule. Actually, any activity coefficient model, for instances NRTL, Wilson, or UNIFAC, can be used to calculate g^{E}. The binary interaction parameters of the NRTL model are treated as regressed parameters for the VLE correlation. The PR-MC-vdW and PR-MC-MHV2 models applied in this work have been described in our previous publications, more details about this model can be found in Appendix SB of *Supplementary Information* or

in references (Yang et al., 2020). The binary interaction parameter k_{ij} of vdW mixing rule and interaction energy parameters Δg_{12} and Δg_{21} of NRTL equation are determined by fitting bubble pressure to the following Objective Function (Eq.13):

$$OF = \frac{100}{N}\sum_{i}^{N}\left(\frac{p_{i,exp} - p_{i,cal}}{p_{i,exp}}\right)^2 \quad (13)$$

The Critical properties and coefficients of Mathias-Copeman alpha function used in this work are listed in Table 2. The Critical properties of R1243zf, R1234yf are taken from REFPROP 10.0 (Lemmon et al., 2018) and that of R245cb are taken from Weber and Defibaugh (1996). The Mathias-Copeman alpha function coefficients (m_1, m_2, and m_3) for R1243zf, R1234yf and R245cb are taken from our previous work (Valtz et al., 2019; Yang et al., 2020).

Table 2. Critical properties and coefficient of Mathias-Copeman alpha function for R1243zf, R1234yf and R245cb.

Components	Critical properties			Mathias-Copeman coefficients		
	T_c/K	p_c/MPa	ω	m_1	m_2	m_3
R1243zf	376.93 [a]	3.5182 [a]	0.261 [a]	0.80529 [c]	-0.57580 [c]	1.64180 [c]
R1234yf	367.85 [a]	3.3822 [a]	0.276 [a]	0.8049 [d]	-0.4242 [d]	1.7469 [d]
R245cb	380.38 [b]	3.1483 [b]	0.297 [b]	0.8920 [d]	-1.2280 [d]	4.7966 [d]

[a] REFPROP 10.0 (Lemmon et al., 2018)
[b] Weber and Defibaugh (1996)
[c] Yang et al.(2020)
[d] Valtz et al. (2019)

4 Results and discussion

4.1 Vapor-liquid coexistence curves

The vapor-liquid coexistence curves of pure R1243zf, R1234yf + R1243zf and R1243zf + R245cb binaries are measured by observing the meniscus and critical opalescence. The experimental results are presented in Tables 3 and Tables 5-8. Symbol *T*, *p*, and ρ represent temperature, pressure, and density, respectively; n is the number of repeated measurements; $\delta(T)$ and $\delta(p)$ are the uncertainties of repeatability for temperature and pressure

measurement respectively, which represent the measurement errors caused by visual observation.

The critical point can be determined through two methods by using the static-synthetic apparatus. The first one is the visual method (Akasaka et al., 2013; Higashi et al., 2015; Juntarachat et al., 2012). If the sample of the desired mass is loaded into the optical cell at critical density, the critical point can be determined by visual observation. The second one is the proposed modeling method which determined the critical point by modelling the vapor -liquid coexistence points to the combined equations of the asymptotic law and rectilinear diameters law. For the measurement of R1243zf, both two methods are utilized to determine the critical point. Seven densities in vapor-phase and eight densities in liquid-phase are obtained in the temperature range from 371.79 to 376.93 K as listed in Table 3. The critical opalescence is observed at three densities of 379.3, 419.6, and 451.5 kg/m^3 (marked with an asterisk in Table 3). At the densities of 379.3 and 451.5 kg/m^3, critical opalescence occurs only in the vapor or liquid phase, but at density of 419.6 kg/m^3 the critical opalescence is observed simultaneously in both vapor and liquid phases, and the intensity of critical opalescence is the strongest compare with the other densities. According to the criteria of visual method (Akasaka et al., 2013; Higashi et al., 2015; Juntarachat et al., 2012; Soo et al., 2010), the density of 419.6 kg/m^3 is considered to be very close to the critical density. Finally, the critical properties of R1243zf are determined to be T_c = 376.50 K, P_c = 3.517 MPa, and ρ_c = 419.6 kg/m^3 based on the visual method.

By contrast, the saturated densities of R1243zf are correlated to the combined equations of the asymptotic law and rectilinear diameters law by proposed modeling method. The critical properties T_c, p_c, and ρ_c of R1243zf are treated as adjusted parameters, and the optimal values are found to be 376.66 K, 3.518 MPa, and 419.0 kg/m^3. The experimental data and modeling results are also shown in Fig. 5. The critical properties determined by the modeling method are quite agreed with those determined by the visual method. Obtaining the critical density by visual method requires multiple adjustments of the sample mass loaded into the critical cell, which is a time-consuming process. The advantage of the proposed modeling method is that it provides a way to accurately determine the critical point and avoids the time-consuming process. Thus, in this work, the critical properties of investigated systems are

taken from the modeling method rather than the visual method.

Table 3. Saturated vapor density and saturated liquid density of R1243zf [a]

Phase	T/K	p /MPa	ρ/kg·m^{-3}	n	δT/K [a]	δp /MPa [b]	U(ρ)/kg·m^{-3}
Saturated vapor phase	372.38	3.244	245.3	9	0.05	0.003	1.3
	375.41	3.439	300.1	6	0.08	0.004	1.6
	376.11	3.487	329.9	5	0.01	0.001	1.7
	376.50*	3.515*	379.3*	6	0.02	0.002	2.0
	374.43	3.374	273.9	6	0.05	0.002	1.4
	376.43	3.510	359.4	4	0.03	0.002	1.9
	374.01	3.347	262.6	4	0.01	0.001	1.4
Saturated liquid phase	376.50*	3.517*	419.6*	7	0.08	0.005	2.2
	376.46	3.516	450.8	6	0.01	0.001	2.3
	376.47*	3.518*	451.5*	6	0.02	0.003	2.3
	376.14	3.495	518.5	6	0.02	0.002	2.7
	375.51	3.451	562.9	5	0.03	0.002	2.9
	371.79	3.218	619.7	5	0.06	0.007	3.2
	376.02	3.472	548.8	5	0.02	0.002	2.7
	373.72	3.368	626.1	4	0.02	0.001	3.0
	372.57	3.290	527.5	5	0.02	0.003	3.2

*Critical opalescence was observed

[a]Extended uncertainty (k=2), U(T)= 0.17 K; U(p)= 0.014 MPa; U(ρ)= 6.4 kg·m^{-3}

[a] $\delta T = \sqrt{\frac{1}{(N-1)}\sum_{i=1}^{N}\left(T_i - T_{avg}\right)^2}$; $T_{avg} = \frac{1}{n}\sum_{i=1}^{n} T_i$

[b] $\delta P = \sqrt{\frac{1}{(N-1)}\sum_{i=1}^{N}(P_i - P_{avg})^2}$; $P_{avg} = \frac{1}{n}\sum_{i=1}^{n} P_i$

Table 4. Available critical properties for R1243zf

Authors	ρ_c/kg·m^{-3}	T_c/K	p_c/MPa
Daubert et al. (1987)	-	378.59	3.609
Higashi et al. (2018)	414	376.93	3.518
Di Nicola et al. (2013)	422.58	378.59	3.6306
REFPROP 10.0 (Lemmon et al., 2013)	413.02	376.93	3.518
This work[a]	419.0	376.66	3.518

[a]Extended uncertainty (k=2), U(T)= 0.17 K; U(p)= 0.014 MPa; U(ρ)= 6.4 kg·m^{-3}

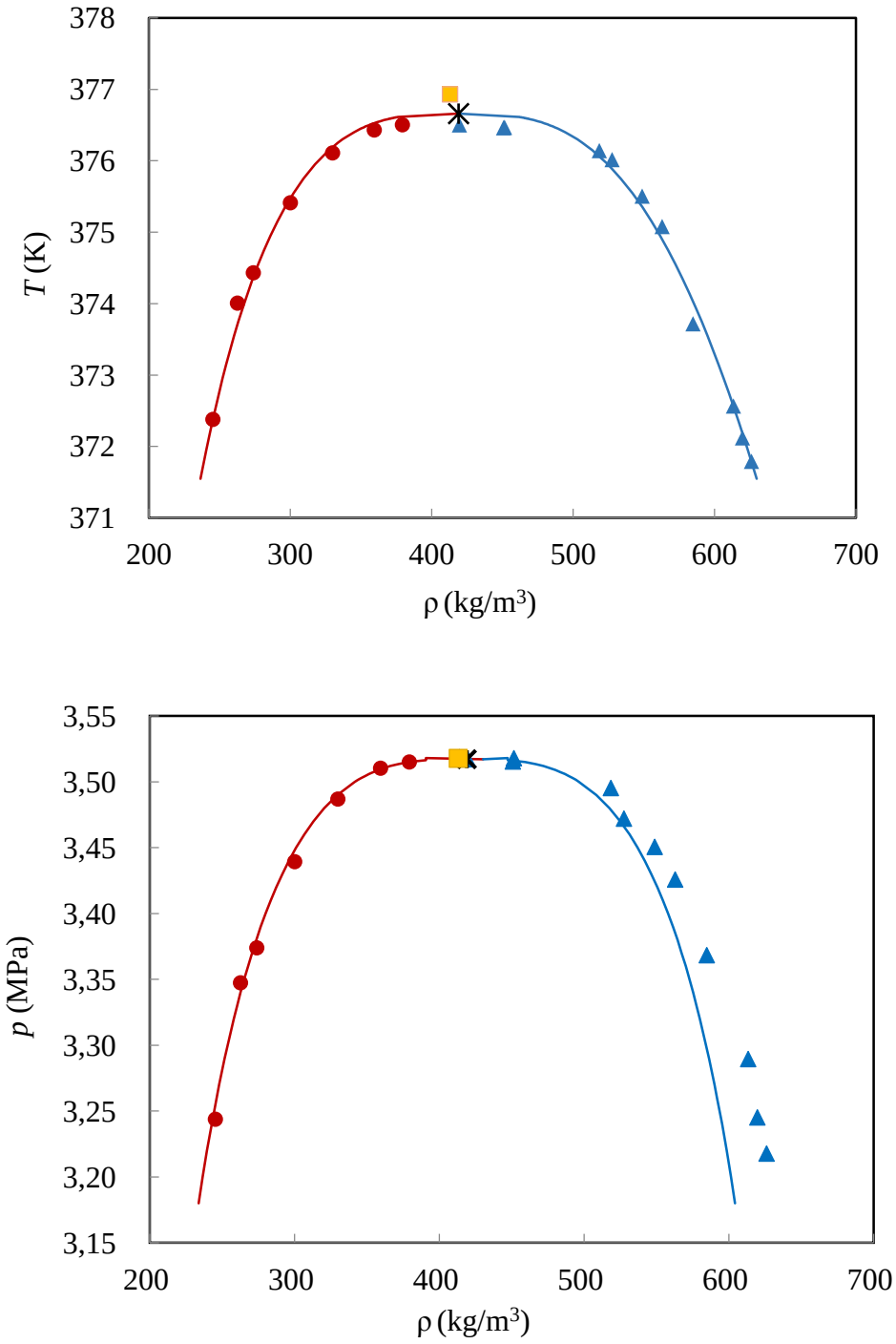

Figure 5. Experimental saturated densities and modeling results of R1243zf in the critical region. (●): vapor phase; (▲): liquid phase; (*): critical point of this work; (■): critical point of REFPROP 10.0; solid lines: combined equations of scaling law and rectilinear diameters law.

To our knowledge, few sets of critical properties of R1243zf have been published in the open literature. The previously reported values are summarized in Table 4. Daubert et al. (1987) published the T_c, and p_c, in 1987 without the detailed information of critical point

determination. Di Nicola et al. (2013) refer to the T_c of Daubert et al. (1987) and p_c of Brown et al. (2013), and present ρ_c by the group contribution method. Therefore, these data resources are taken less consideration. The T_c of this work is consistent with that of Higashi et al. (2018) and the value of REFPROP 10.0 (Lemmon et al., 2018), while the reported T_c of Daubert et al. (Daubert and Hutchison, 1990) is higher than other's. The p_c of this work is very agree with that of Higashi et al (2018) and the value of REFPROP 10.0, while the reported p_c of Di Nicola et al. (2013) and Daubert et al. (1987) exhibit positive error of 0.1 MPa. The ρ_c reported in the literature is close to each other, especially the value of Higashi et al. (2018) and REFPROP 10.0. The ρ_c of this work is consistent with REFPROP 10.0 with positive error of 5.98 kg/m^3.

For the critical point measurement of mixture, the measurement procedure is quite similar to that of pure R1243zf. The difference is that the mixture needs to be prepared and loaded (keep the composition unchanged) into the optical cell and the selection of the right pressure transducer for measurement of vapor or liquid phase densities. The R1243zf + R1234yf binary mixture is prepared at three different mole fractions of 0.2774, 0.4954, and 0.7509, and the R1243zf + R245cb binary is prepared at mole fraction of 0.4971.

The critical point of mixture is not determined by the visual method but the modeling method. The vapor-liquid coexistence curves of R1243zf (1) + R1234yf (2) binary at three mole fractions were measured in temperature range of 363.24 to 373.97 K as summarized in Tables 5 - 7, and the experimental temperatures, pressures, and saturated densities are correlated to the combined equations of the asymptotic law and rectilinear diameters law. The determined T_c, p_c, and ρ_c of R1243zf (1) + R1234yf (2) binary for each composition is listed in Table 10. For each composition, sixteen saturated densities were obtained. The critical opalescence is observed at the densities marked with asterisks.

Fig 6 shows the vapor-liquid coexistence curve of R1243zf (1) + R1234yf (2) along with that of pure R1243zf and R1234yf. Whether it is the experimental data of this work or the data of REFPROP 10.0, it was found that the p - ρ curves of R1243zf intersected with that of R1234yf, and the p - ρ curves of R1243zf+R1234yf mixture intersected with both pure R1243zf and R1234yf. This suggests that the p - ρ curve intersection is characteristic of the mixture itself and not due to measurement error. The T - ρ curves of R1243zf (1) + R1234yf

(2) binary show parallel lines in the experimental range, but in theory, it will intersect somewhere. The regressed critical points are almost at the maximum for the T - ρ or p - ρ curves. However, it is not the case for the p - ρ curve on mole fraction of 0.4954. At the densities of 411.2 and 439.8 kg·m^{-3}, their pressure deviations on repeated measurement are 0.012 and 0.013 MPa respectively, resulting in big errors with the modeling p - ρ curve. Therefore, for this p - ρ curve, the critical pressure lower than the maximum pressure is caused by the error of pressure measurement. Besides, the pure R1243zf p - ρ curve of this work does not well agreed with that of REFPROP 10.0, more experimental data are needed to verify the experimental results.

The critical properties of the R1243zf (1) + R1234yf (2) binary mixture is correlated using the Redlich-Kister type equation as following Eqns. (14), (15) and (16). The critical properties T_c, p_c, and ρ_c of the binary mixture can be regarded as the sum of ideal contributions (the first two terms) and non-ideal contribution (summation term).

$$T_{c,mix}(K) = x_1 T_{c,1} + x_2 T_{c,2} + \sum_{j=1}^{n} a_j x_1 x_2 (2x_1 - 1)^{j-1} \quad (14)$$

$$p_{c,mix}\,(MPa) = x_1 P_{c,1} + x_2 p_{c,2} + \sum_{j=1}^{n} b_j x_1 x_2 (2x_1 - 1)^{j-1} \quad (15)$$

$$v_C\left(\frac{m^3}{kg}\right) = {}^{1}\!/_{\rho_{c,mix}\,(kg/m^3)} = x_1 \frac{1}{\rho_{c,1}} + x_2 \frac{1}{\rho_{c,2}} + \sum_{j=1}^{n} c_j x_1 x_2 (2x_1 - 1)^{j-1} \quad (16)$$

where $T_{c,mix}$, $p_{c,mix}$, and $\rho_{c,mix}$ are the critical temperature, pressure, and density of the binary mixture; $T_{c,i}$, $p_{c,i}$, and $\rho_{c,i}$ are the critical temperature, pressure, and density for pure component i; n is the number of coefficients, n=3; a_j, b_j and c_j are the empirical coefficients which are determined by minimizing the relative mean standard deviation (RMSD):

$$\text{RMSD} = \sqrt{\left[\frac{1}{N}\sum_{j}(M_{exp} - M_{cal})_j^2\right]} \quad (17)$$

where $M = T_c$ or p_c, and N is the number of data points.

The experimental and correlated binary critical properties T_c, p_c, and ρ_c are plotted in Figure 7. The coefficients for each binary system are listed in Table 9.

Table 5. Saturated vapor density and saturated liquid density of R1243zf + R1234yf binary mixture at mole fraction of 0.2774

Phase	T/K	p /MPa	ρ/kg·m^{-3}	n	δT/K	δp /MPa	U(ρ)/kg·m^{-3}
Saturated vapor phase	367.45	3.264	293.9	6	0.09	0.005	1.3
	369.02	3.374	343.7	4	0.01	0.001	1.5
	369.55	3.412	388.7	5	0.02	0.001	1.7
	369.61*	3.417*	425.3*	5	0.01	0.001	1.9
	368.11	3.310	312.2	6	0.04	0.002	1.4
	368.47	3.335	323.1	5	0.02	0.001	1.4
	369.31	3.394	362.1	5	0.01	0.001	1.6
	369.53	3.410	389.4	5	0.01	0.001	1.7
Saturated liquid phase	369.61*	3.422*	482.4*	5	0.01	0.002	2.1
	369.54	3.417	519.7	5	0.01	0.001	2.0
	368.96	3.379	576.4	5	0.02	0.001	2.5
	367.72	3.296	617.7	5	0.04	0.003	2.7
	369.58	3.420	499.4	6	0.01	0.001	2.1
	369.37	3.406	545.4	4	0.01	0.001	2.3
	368.49	3.347	593.7	5	0.02	0.002	2.5
	367.24	3.269	627.7	4	0.01	0.008	2.7

*Critical opalescence was observed

[a] Extended uncertainty (k=2), U(T)= 0.19 K; U(p)= 0.016 MPa; U(ρ)= 6.4 kg·m^{-3}; U(x_1) =1.8×10^{-4}

Table 6. Saturated vapor density and saturated liquid density of R1243zf + R1234yf binary mixture at mole fraction of 0.4954

Phase	T/°K	p /MPa	ρ/kg·m^{-3}	n	δT/K	δp /MPa	U(ρ)/kg·m^{-3}
Saturated vapor phase	367.78	3.192	260.4	5	0.04	0.022	1.1
	370.64	3.390	311.4	6	0.10	0.024	1.3
	371.46	3.440	384.0	5	0.01	0.004	1.6
	371.50	3.454	411.2	6	0.01	0.012	1.7
	371.50	3.457	439.8	5	0.01	0.013	1.8
	368.38	3.226	269.9	5	0.08	0.004	1.1
	369.38	3.294	287.9	5	0.07	0.003	1.3
	371.23	3.422	346.5	5	0.05	0.003	1.5
	371.46*	3.441*	393.0*	4	0.02	0.001	1.7
Saturated liquid phase	371.51	3.450	466.8	5	0.03	0.002	1.8
	371.49	3.450	509.1	5	0.06	0.004	1.9
	371.23	3.432	548.3	5	0.01	0.001	2.1
	370.38*	3.375*	592.0*	5	0.03	0.002	2.3
	368.28	3.239	643.4	5	0.03	0.022	2.5
	371.54	3.452	503.8	4	0.04	0.003	1.9
	371.17	3.429	557.8	5	0.02	0.002	2.1

*Critical opalescence was observed

[a]Extended uncertainty (k=2): U(T)= 0.21 K, U(p)= 0.048 MPa, U(ρ)= 6.4 kg·m^{-3}, U(x_1) =5.8×10^{-5}

Table 7. Saturated vapor density and saturated liquid density of R1243zf + R1234yf binary mixture at mole fraction of 0.7509

Phase	T/K	p/MPa	ρ/kg·m^{-3}	n	δT/K	δp /MPa	U(ρ)/kg·m^{-3}
Saturated vapor phase	371.38	3.298	269.6	5	0.04	0.002	1.2
	373.53	3.448	329.6	4	0.02	0.001	1.6
	373.93	3.477	371.8	5	0.02	0.001	1.8
	373.97*	3.481*	411.0*	5	0.01	0.001	2.0
	372.17	3.355	286.8	4	0.01	0.001	1.4
	372.73	3.393	300.0	5	0.02	0.002	1.5
	373.64	3.456	337.0	5	0.03	0.002	1.6
	373.81*	3.469*	353.2*	4	0.01	0.001	1.7
Saturated liquid phase	373.94*	3.483*	443.7*	4	0.01	0.001	1.8
	373.93	3.483	483.2	5	0.03	0.002	2.0
	373.70	3.468	528.6	5	0.02	0.001	2.2
	373.14	3.431	563.1	5	0.01	0.001	2.3
	373.93	3.483	451.5	6	0.02	0.001	1.9
	373.82	3.477	504.7	5	0.02	0.001	2.1
	371.99	3.356	592.8	5	0.05	0.000	2.5
	372.54	3.391	577.0	5	0.02	0.002	2.4

*Critical opalescence was observed

[a]Extended uncertainty (k=2): U(T)= 0.11 K, U(p)= 0.004 MPa, U(ρ)= 6.4 kg·m^{-3}, U(x_1) =5.8×

10^{-5}

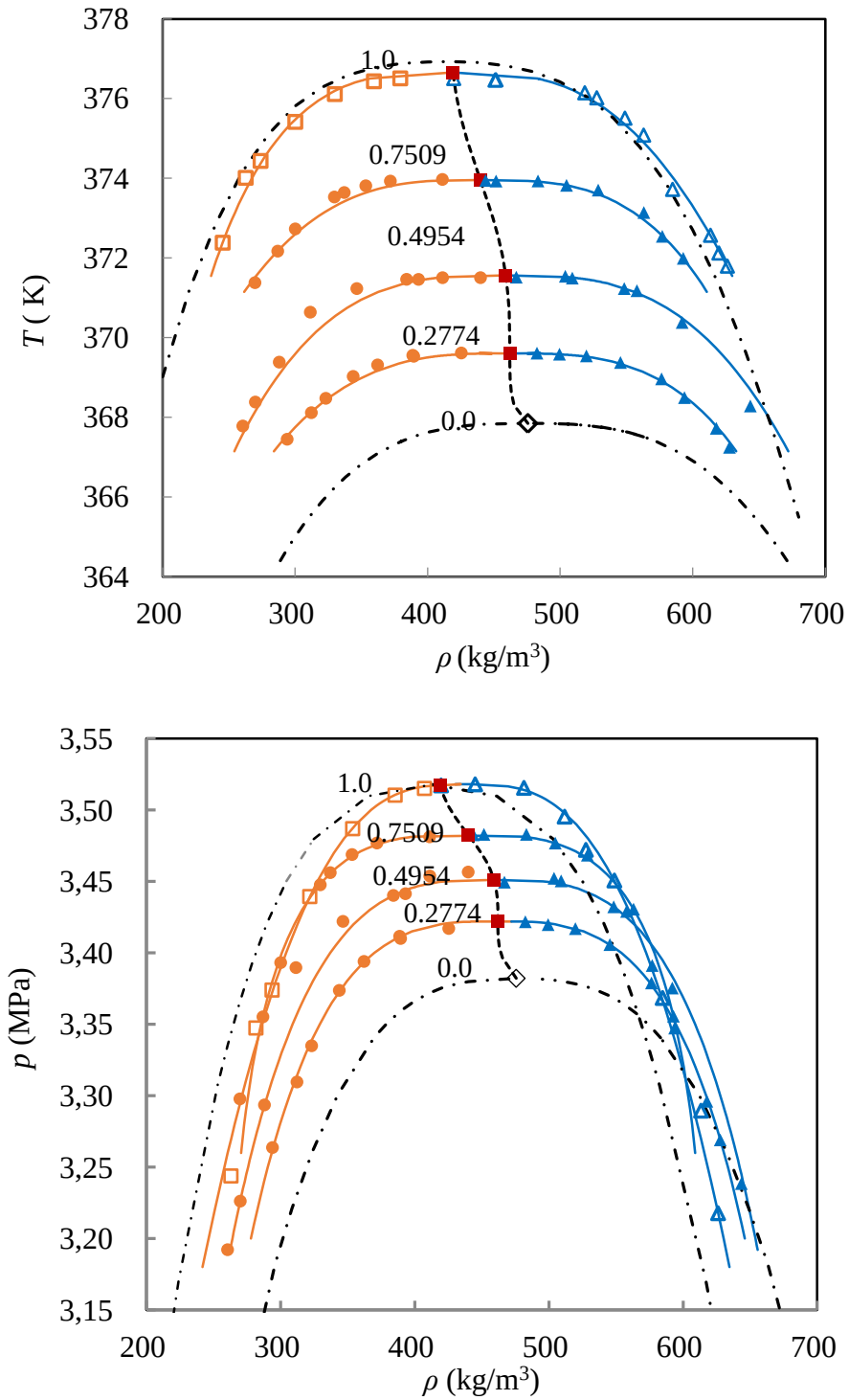

Figure 6. Vapor-liquid coexistence curves of R-1243zf (1) + R-1234yf (2) mixtures. (□): vapor phase R1243zf; (△): liquid phase R1243zf; (●) saturated vapor phase of R1243zf + R1234yf mixture; (▲): saturated liquid phase of R1243zf + R1234yf mixture; (■): critical point of this work; (◊): critical point of R1234yf from REFPROP 10.0; solid lines: combined equations of scaling law and rectilinear diameters law; dash lines: vapor-liquid coexistence curves of R1234yf and R1243zf from REFPROP 10.0; dot line: critical line calculated by Redlich-Kister equation.

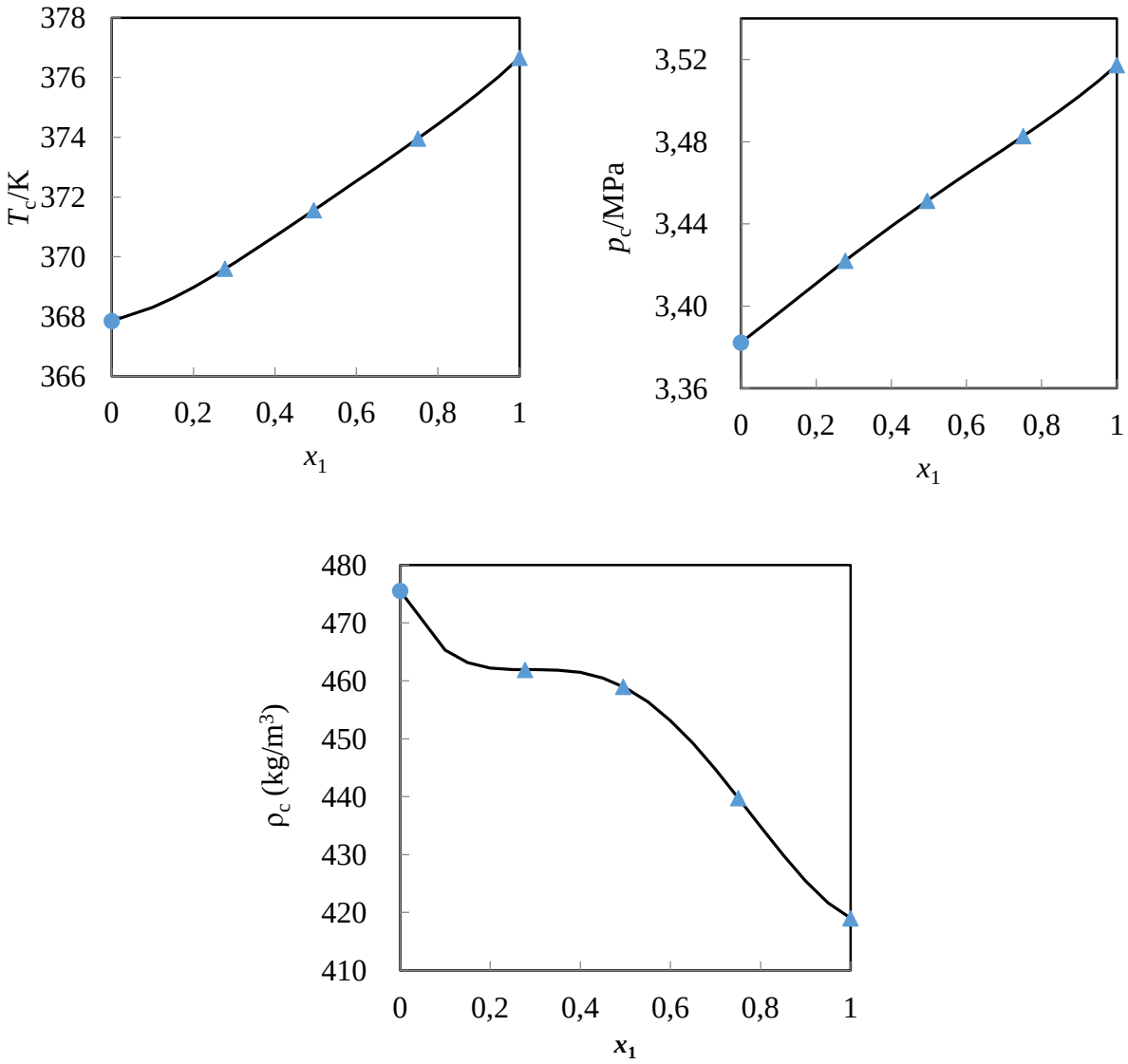

Figure 7. Experimental critical pressures and temperatures for the R1243zf (1) + R1234yf (2) system. (●) critical point of R1234yf from REFPROP 10.0; (▲): critical point of R1243zf (1) + R1234yf (2) binary system in this work; solid lines: Redlich–Kister correlation.

The vapor-liquid coexistence curve of R1243zf (1) + R245cb (2) binary system was measured with mole fraction of 0.4971. Experimental data are summarized in Table 8. Six densities in vapor-phase and four densities in liquid-phase were obtained in the temperature range of 369.54 - 377.36 K. The determined T_c, p_c, and ρ_c of R1243zf (1) + R245cb (2) binary system are lists in Table 10. The T - ρ curve and p - ρ curve of R1243zf (1) + R245cb (2) binary system along with that of pure R1243zf and R245cb are shown in Fig.8. Due to the lack of sufficient samples of R245cb, we failed to complete the measurement of vapor-liquid

coexistence curve for pure R245cb. Therefore, we use literature data to observe the relationship of the critical properties and the composition for R1243zf (1) + R245cb (2) binary system.

To our knowledge, Shank (1967) presented critical parameters and saturated properties of R245cb in 1967. The critical properties (T_c =380.11 K, p_c = 3.137 MPa, and ρ_c = 498.8 kg/m^3) were determined graphically from large-scale plots of P-V-T data, and the saturated liquid and vapor densities were generated from BWR equation of state. Weber and Defibaugh (1996) presented vapour pressure of R245cb in 1996, and they used T_c =380.38 K and ρ_c = 498.8 kg/m^3 for regression of vapour pressure equation. Those critical parameters of R245cb were private communicated with Schmidt, NIST in 1995. Defibaugh and Moldover (1997) presented saturated liquid density equations of R245cb in 1997, and they also adopted Schmidt's critical parameters for data regression. Therefore, T_c =380.38 K and ρ_c = 498.8 kg/m^3 from Schmidt's critical parameters, and p_c = 3.1483 MPa from Weber's Wagner equation (Weber and Defibaugh, 1996) are utilized in this work. The generated saturated densities in critical region (3 in vapor phase, and 3 in liquid phase) of Shank (1967) are agree with saturated liquid density equation of Defibaugh and Moldover (1997) as displayed in Fig. 8. Hence, those two data sets are utilized as well. However, it is difficult to observe the relationship between the critical parameters and the molar fraction for the R1243zf (1) + R245cb (2) system due to the lack of enough data for the mixture.

Table 8. Saturated vapor density and saturated liquid density of R1243zf + R245cb binary mixture at composition of 0.4971 [a]

Phase	T/K	p/MPa	ρ/kg·m^{-3}	n	δT/K	δp/MPa	U(ρ)/kg·m^{-3}
Vapor phase	369.54	2.829	225.0	7	0.08	0.002	0.9
	373.03	3.024	261.5	5	0.05	0.001	1.0
	375.82	3.198	309.8	5	0.03	0.001	1.2
	377.33*	3.303*	442.8*	6	0.01	0.001	1.7
	377.30	3.298	391.1	6	0.01	0.001	1.5
	377.34	3.302	414.7	4	0.01	0.002	1.6
Liquid phase	377.36	3.296	484.5	6	0.01	0.001	1.9
	377.33	3.295	537.2	5	0.02	0.002	2.0
	375.90	3.207	619.5	5	0.03	0.001	2.3
	370.49	2.890	712.9	5	0.03	0.001	2.7

*Critical opalescence was observed

[a]Extended uncertainty (k=2): U(T)= 0.17 K, U(p)= 0.004 MPa, U(ρ)= 6.4 kg·m^{-3}, U(x_1) =5.8×10^{-5}

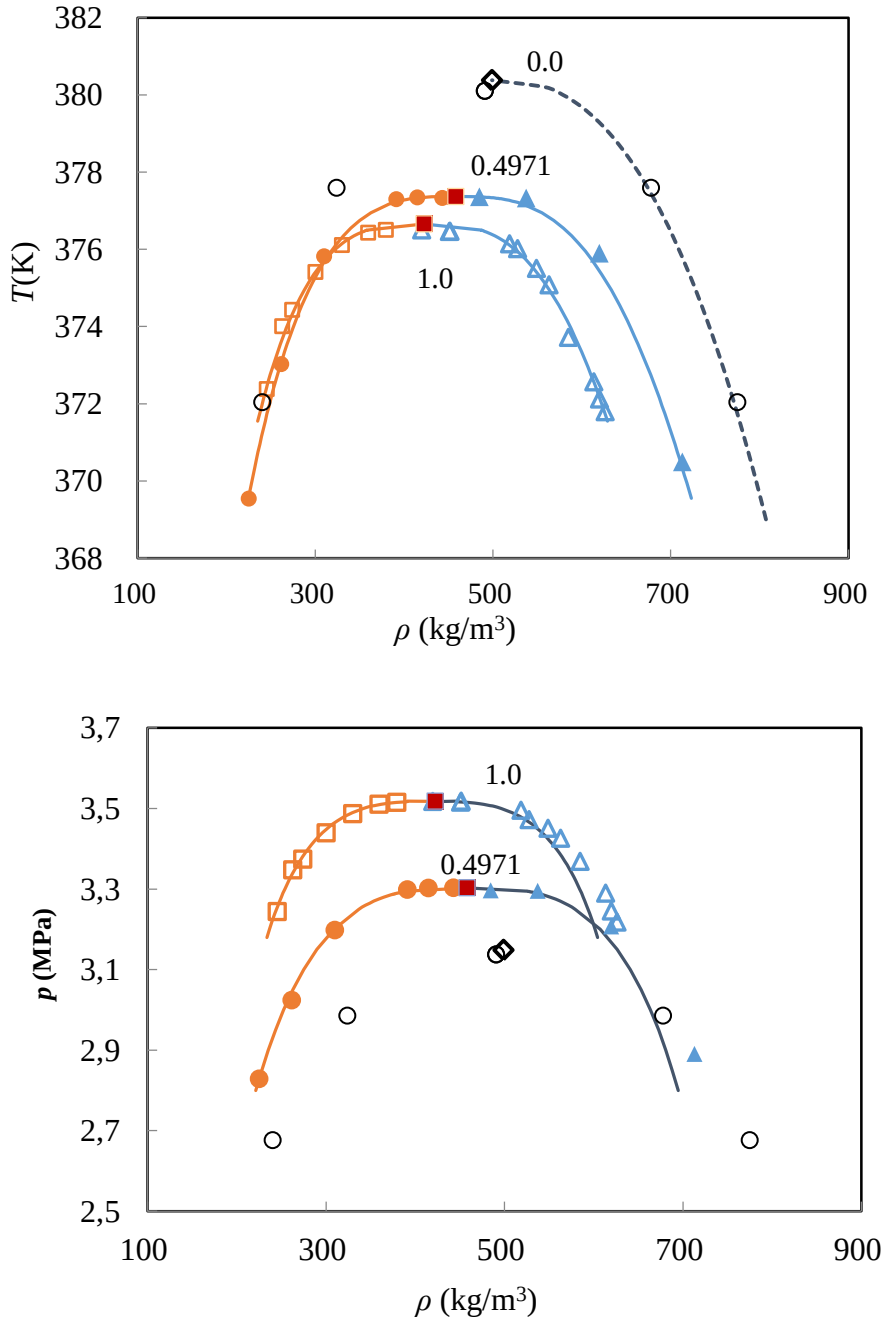

Figure 8. Vapor-liquid coexistence curves of R1243zf (1) + R-245cb (2) mixtures. (□): vapor phase R1243zf ; (△): liquid phase R1243zf; (●) saturated vapor phase of R1243zf + R-245cb mixture; (▲): saturated liquid phase of R1243zf + R-245cb mixture; (■): critical point of this work; (◊): critical point of R245cb from literature (Weber and Defibaugh, 1996)(Defibaugh and Moldover, 1997); (○): generated saturated density of R245cb from BWR equation (Shank, 1967). solid lines: combined equations of asymptotic law behavior and rectilinear diameters law; dash lines: saturated liquid density of R245cb from Defibaugh and Moldover (1997);

Table 9. The Redlich–Kister constants for Eqns. (14), (15) and (16) for the R1243zf+R1234yf binary mixtures in this work.

System	Regressed constants		
	Eq. (14)		
	a_1/K	a_2/K	a_3/K
	-2.606	0.894	-2.234
	Eq. (15)		
R1243zf+R1234yf	b_1/MPa	b_2/MPa	b_3/MPa
	0.008	-0.017	-0.019
	Eq. (16)		
	c_1/kg·m^{-3}	c_2/kg·m^{-3}	c_3/kg·m^{-3}
	-2.61×10^{-4}	-1.78×10^{-4}	4.97×10^{-4}

Table 10. The correlated critical properties and constants of investigated systems from the combined equations of asymptotic law behavior and rectilinear diameters law.

x_1	ρ_c/ kg·m^{-3}	T_c/K	p_c/MPa	*A*	*B*	*C*	*D*
R1243zf							
1	419.0	376.66	3.517	-2.7799	231.442	0.1488	0.7010
R1243zf + R1234yf							
0.7509	439.8	373.96	3.483	1.2809	249.598	0.4671	0.7963
0.4954	459.0	371.56	3.451	-0.9424	258.167	0.0126	0.3383
0.2774	461.9	369.60	3.422	1.4277	260.752	0.0135	0.3306
R1243zf + R245cb							
0.4971	458.0	377.37	3.303	-2.0564	255.335	0.0849	0.6996

[a] Extended uncertainty (k=2): U(*T*)= 0.10 K,U(*p*)= 0.042 MPa,U(ρ)= 6.4 kg·m^{-3},U(x_1) = 5.8×10^{-5}

3.2 Vapor liquid equilibrium

Saturated vapor pressures of pure R1243zf, R1234yf, and R245cb were measured by using PVT apparatus at four temperatures of 293.45, 313.47, 333.46, and 353.55 K. The results are presented in Table 11. The vapor pressure of the three pure compounds was obtained from the break point of *P*-V_T curve. The vapor pressures of R1243zf and R1234yf were compared with calculated values of REFPROP 10.0, and the vapor pressures of R245cb were compared with vapor pressure equation of Valtz et al. (2019). The absolute deviations (*Δp*) between measured vapor pressures and calculated values are within ± 0.017 MPa. Considering the extended uncertainty of pressure measurement for PVT apparatus is 0.015 MPa, the measured results are correct and reliable.

Table 11. Experimental and calculated vapor pressures of pure components [a].

Component	*T*/K	p_{exp}/MPa	p_{ref}/MPa	Δp[d]/MPa	δp[e] /%
R1243zf	293.45	0.518	0.515 [b]	0.003	0.65
	313.38	0.891	0.890 [b]	0.001	0.16
	333.43	1.436	1.442 [b]	-0.006	-0.41
	353.54	2.203	2.211 [b]	-0.008	-0.34
R1234yf	293.42	0.596	0.596 [b]	-0.004	-0.69
	313.40	1.042	1.025 [b]	0.017	1.67
	333.49	1.664	1.655 [b]	0.010	0.57
	353.57	2.532	2.541 [b]	-0.009	-0.37
R245cb	293.45	0.409	0.403 [c]	0.006	1.47
	313.47	0.731	0.715 [c]	0.016	2.23
	333.46	1.170	1.176 [c]	-0.006	-0.51
	353.55	1.816	1.833 [c]	-0.017	-0.94

[a] Extended uncertainty (k=2), U(T)= 0.06 K; U(P)= 0.015 MPa

[b] REFPROP 10.0 (Lemmon et al., 2018)

[c] Valtz et al. (2019).

[d] $\Delta p = p_{exp} - p_{ref}$

[e] $\delta p = 100 \times (p_{exp} - p_{ref})/p_{exp}$.

The bubble pressures of R1243zf + R1234yf and R1243zf + R245cb binary systems with three different compositions were measured by using the PVT apparatus in the range of 293.45 to 353.55 K. Table 12 and Table 13 show the experimental bubble pressures of the two binaries. *T* and *p* represent the experimental temperature and pressure; n is the number of repeated measurements; x_1 are the liquid phase mole fraction; $\delta(T)$ and $\delta(p)$ are the uncertainty of measurement repeatability for temperature and pressure respectively; p_{cal} and $y_{1.cal}$ represent the calculated value of pressure and vapor phase mole fraction from selected cubic EoS respectively; Δx_1 are the uncertainty of liquid phase mole fraction.

The bubble pressures of R1234yf +R1243zf and R1243zf + R245cb systems are correlated by PR-MC-vdW and PR-MC-MHV2 models respectively. The regressed binary interaction parameter k_{12} of vdW mixing rules and interaction energy parameters Δg_{12} and Δg_{21} of MHV2 mixing rules are presented in Table 14. The vapor liquid equilibrium (VLE) of the R1243zf + R1234yf and R1243zf + R245cb systems are predicted by PR-MC-vdW and PR-MC-MHV2 models respectively, and the phase diagrams are illustrated in Figs 9 and 11.

The vapor phase line is very close to the liquid phase line at each investigated temperature for the two binary systems. The two systems show near-azeotropic phase behavior with slightly positive deviations from ideality, and the phase diagrams are very similar to previous studied R1243zf + R1234ze(E) system (Yang et al., 2020). The systems of R1234yf +R1243zf and R1243zf + R245cb show type I phase behavior based on the classification scheme of van Konynenburg and Scott (1980) (Coquelet and Richon, 2009).

The phase curves displayed by the PR-MC-vdW and PR-MC-MHV2 models are almost the same, as shown in Figs 9 and 11. In order to further analyze the correlation results, the pressure deviations of two models are presented in Figs 10 and 12. Both the two models show almost the same deviations at each isothermal.

The average relative deviation of pressure (*ARDP*) and the average bias of pressure (*BIASP*) are defined to evaluate the accuracy of the two models:

$$ARDP = \frac{100}{N}\sum_{i=1}^{N}\frac{\left|P_{i,exp} - P_{i,cal}\right|}{P_{i,exp}} \tag{18}$$

$$BIASP = \frac{100}{N}\sum_{i=1}^{N}\frac{P_{i,exp} - P_{i,cal}}{P_{i,exp}} \tag{19}$$

where N is the number of experimental points, the subscripts *exp* and *cal* represent experimental and calculated pressure respectively.

The calculated *ARDP* and *BIASP* of PR-MC-MHV2 model are identical or smaller than that of PR-MC-vdW model at each isotherm for the two systems as presented in Table 13. Base on the results of calculated *ARDP* and *BIASP* along with the deviation Figs 10 and 12, we can draw the conclusion that the PR-MC-vdW and PR-MC-MHV2models perform almost the same ability in VLE prediction for the two binaries, and the accuracy of the PR-MC-MHV2 model is slightly better.

Furthermore, the isothermal and isobaric VLE properties of R1234yf (1) + R1243zf (2) and R1243zf (1) + R245cb (2) systems are predicted in high temperature region up to mixture critical lines, which is shown in the *Supplementary Information*. There is good agreement as we can see in Figures S2 and S3 between critical point measurement and prediction from thermodynamic model with parameters adjusted on bubble point pressure data.

Table 12. Vapor liquid equilibrium of R1234yf (1) +R1243zf (2) binary system

The experimental data							The calculated results			
							PR-MC-vdW		PR-MC-MHV2	
T/K	δT/K	x_1	$\Delta x_1/(10^{-5})$	P_{exp}/MPa	δP/MPa	n	P_{cal}/MPa	$y_{1.cal}$	P_{cal}/MPa	$y_{1.cal}$
T = 293.44 K										
293.42	0.02	0	-	0.512	0	4	0.512	0	0.512	0
293.41	0.03	0.2057	3.3	0.530	0.001	7	0.530	0.2201	0.517	0.2278
293.51	0.03	0.4874	3.2	0.553	0.003	5	0.553	0.5331	0.544	0.5194
293.42	0.04	0.7229	2.6	0.573	0.001	4	0.573	0.7599	0.575	0.7474
293.45	0.07	1	-	0.596	0.001	4	0.596	1	0.596	1
T = 313.42 K										
313.40	0.06	0	-	0.885	0.002	4	0.885	0	0.885	0
313.31	0.02	0.2057	3.3	0.921	0.001	4	0.913	0.2272	0.921	0.2285
313.30	0.03	0.4874	3.2	0.964	0.001	3	0.963	0.5234	0.964	0.5153
313.41	0.05	0.7229	2.6	0.995	0.008	4	1.003	0.7453	0.995	0.7412
313.44	0.08	1	-	1.025	0.002	4	1.025	1	1.025	1
T = 333.42 K										
333.49	0.08	0	-	1.437	0.002	3	1.437	0	1.437	0
333.29	0.04	0.2057	3.3	1.506	0.004	4	1.494	0.2266	1.506	0.2275
333.36	0.10	0.4874	3.2	1.580	0.002	3	1.579	0.5165	1.580	0.5101
333.46	0.03	0.7229	2.6	1.624	0.003	4	1.637	0.7380	1.624	0.7349
333.52	0.06	1	-	1.656	0.004	6	1.656	1	1.656	1
T = 353.55 K										
353.57	0.03	0	-	2.223	0.005	3	2.223	0	2.223	0
353.74	0.01	0.2057	3.3	2.296	0.007	4	2.294	0.2174	2.296	0.2175
353.33	0.07	0.4874	3.2	2.390	0.002	4	2.390	0.5034	2.390	0.5030
353.58	0.02	0.7229	2.6	2.465	0.002	4	2.467	0.7340	2.465	0.7338
353.54	0.01	1	-	2.550	0.002	2	2.550	1	2.550	1

[a] Extended uncertainty (k=2): U(T)= 0.06 K, U(P)= 0.015 MPa, $U(x_1) = 6.6*10^{-5}$

Table 13. Vapor liquid equilibrium of R1243zf (1) + R245cb(2) binary system

The experimental data							The calculated results			
							PR-MC-vdW		PR-MC-MHV2	
T/K	δT/K	x_1	$\Delta x_1/(10^{-5})$	P_{exp}/MPa	δP/MPa	n	P_{cal}/MPa	$y_{1.cal}$	P_{cal}/MPa	$y_{1.cal}$
T = 293.43 K										
293.45	0.03	0	-	0.410	0.001	5	0.399	0	0.399	0
293.46	0.02	0.4971	3.1	0.482	0.003	3	0.479	0.5516	0.479	0.5437
293.38	0.03	0.7494	3.0	0.496	0.001	4	0.501	0.7723	0.498	0.7709
293.42	0.08	0.2699	3.7	0.450	0.000	3	0.448	0.3321	0.452	0.3294
293.45	0.02	1	-	0.518	0.000	4	0.512	1	0.512	1
T = 313.41 K										
313.47	0.08	0	-	0.731	0.003	4	0.707	0	0.707	0
313.41	0.02	0.4971	3.1	0.835	0.003	3	0.831	0.4971	0.830	0.5342
313.41	0.07	0.7494	3.0	0.858	0.002	4	0.867	0.7494	0.862	0.7675
313.36	0.04	0.2699	3.7	0.787	0.002	4	0.783	0.2699	0.789	0.3173
313.38	0.06	1	-	0.891	0.002	4	0.886	1	0.885	1
T = 333.45 K										
333.46	0.01	0	-	1.155	0.005	4	1.166	0	1.167	0
333.47	0.01	0.4971	3.1	1.323	0.006	4	1.321	0.5325	1.321	0.5292
333.43	0.02	0.7494	3.0	1.379	0.014	4	1.385	0.7707	1.381	0.7701
333.46	0.04	0.2699	3.7	1.260	0.019	4	1.256	0.3032	1.260	0.3021
333.43	0.08	1	-	1.436	0.002	3	1.440	1	1.438	1
T = 353.52 K										
353.55	0.02	0	-	1.806	0.003	4	1.828	0	1.828	0
353.53	0.02	0.4971	3.1	2.038	0.017	4	2.048	0.5224	2.047	0.5272
353.50	0.01	0.7494	3.0	2.163	0.002	3	2.142	0.7650	2.158	0.7666
353.50	0.08	0.2699	3.7	1.946	0.020	2	1.953	0.2934	1.940	0.2942
353.54	0.03	1	-	2.203	0.005	3	2.226	1	2.222	1

[a] Extended uncertainty (k=2): U(T)= 0.06 K, U(P)= 0.015 MPa, $U(x_1) = 7.4*10^{-5}$

Table 14. The binary interaction parameters adjusted by the model stated as above at each temperature

T /K	PR-MC-vdW				PR-MC-MHV2				
	k_{12}	OF	*ARDP*/%	*BIASP*/%	Δg_{12}/J mol^{-1}	Δg_{21}/J mol^{-1}	OF	*ARDP*/%	*BIASP* /%
R1234yf (1) + R1243zf (2)									
293.43	0.000	0.0247	1.41	-0.54	-960.85	1418.55	0.0092	0.86	0.33
313.41	0.005	0.0288	1.61	0.69	-795.98	1121.60	0.0267	1.56	0.67
333.45	0.012	0.0054	0.57	0.14	-765.19	1084.35	0.0031	0.50	0.15
353.52	0.002	0.0027	0.36	-0.32	-407.29	474.26	0.0027	0.33	-0.32
R1243zf (1) + R245cb (2)									
293.43	0.021	0.0188	1.16	0.66	-469.14	706.99	0.0169	1.07	0.68
313.41	0.020	0.0260	1.19	0.75	-564.60	830.13	0.0238	1.03	0.76
333.45	0.008	0.0027	0.39	-0.24	-574.93	750.80	0.0022	0.28	-0.23
353.52	0.007	0.0072	0.78	-0.38	1165.33	-842.11	0.0053	0.62	-0.39

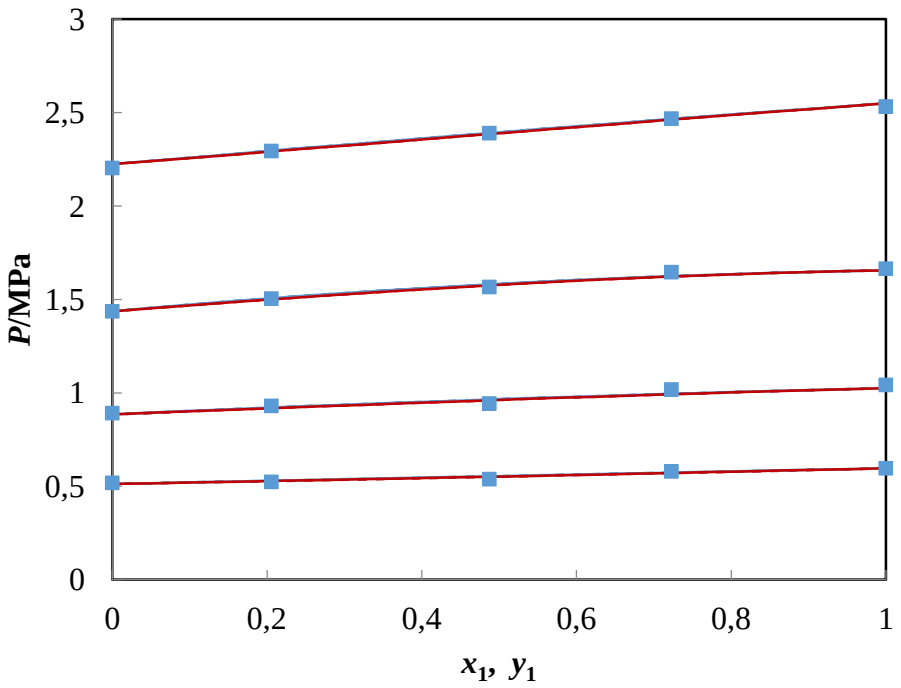

Figure 9. VLE for the R1234yf (1) + R1243zf (2) binary system at four temperatures of 293.44, 313.42, 333.42, 353.55 K. (■): bubble point; dash lines: PR-MC-vdW model; solid lines: PR-MC-MHV2 model.

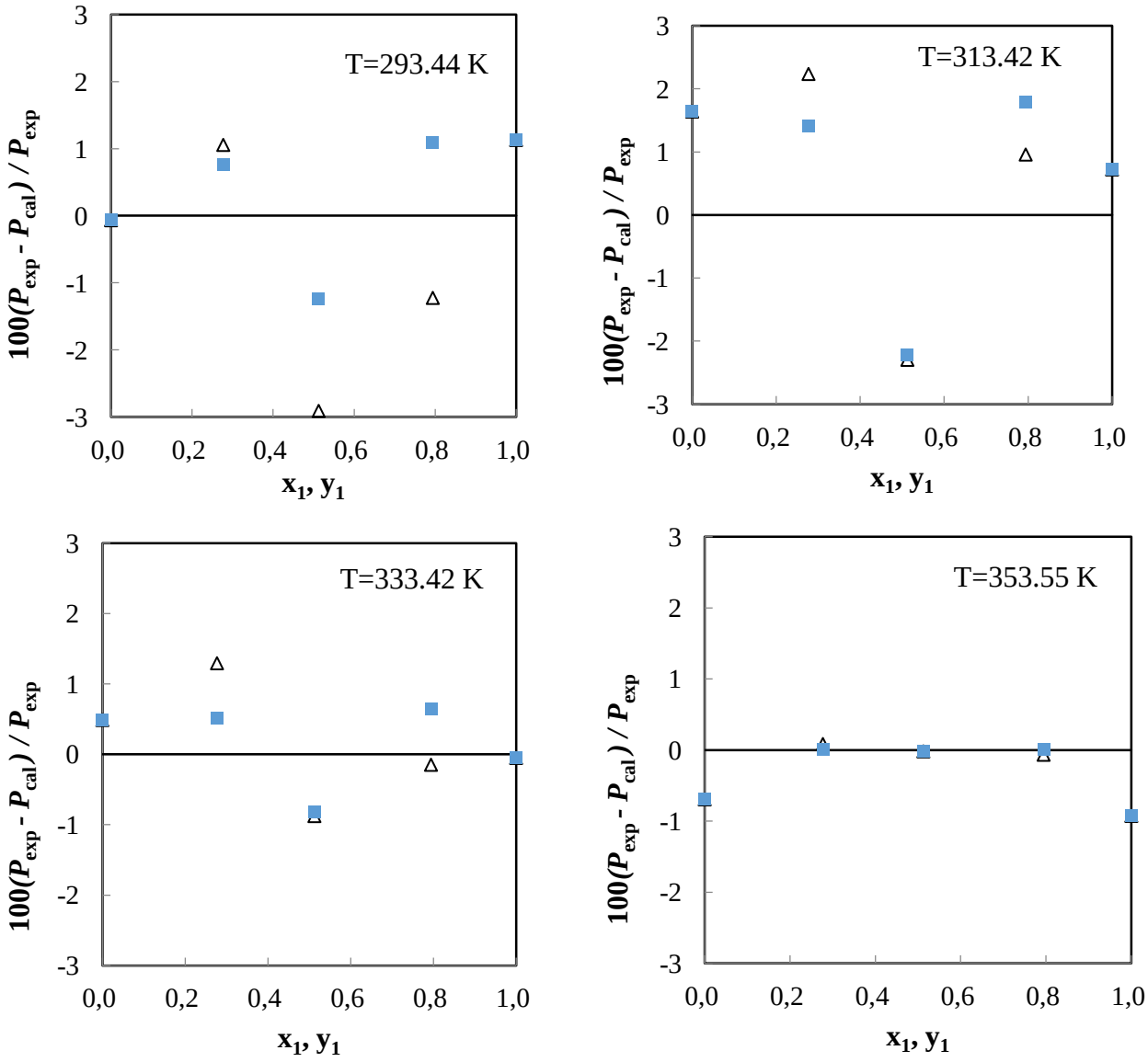

Figure 10. Relative deviation of pressure for the R1234yf (1) + R1243zf (2) binary system from PR-MC-vdW and PR-MC-MHV2 model. (△): PR-MC-vdW model; (■): PR-MC-MHV2 model.

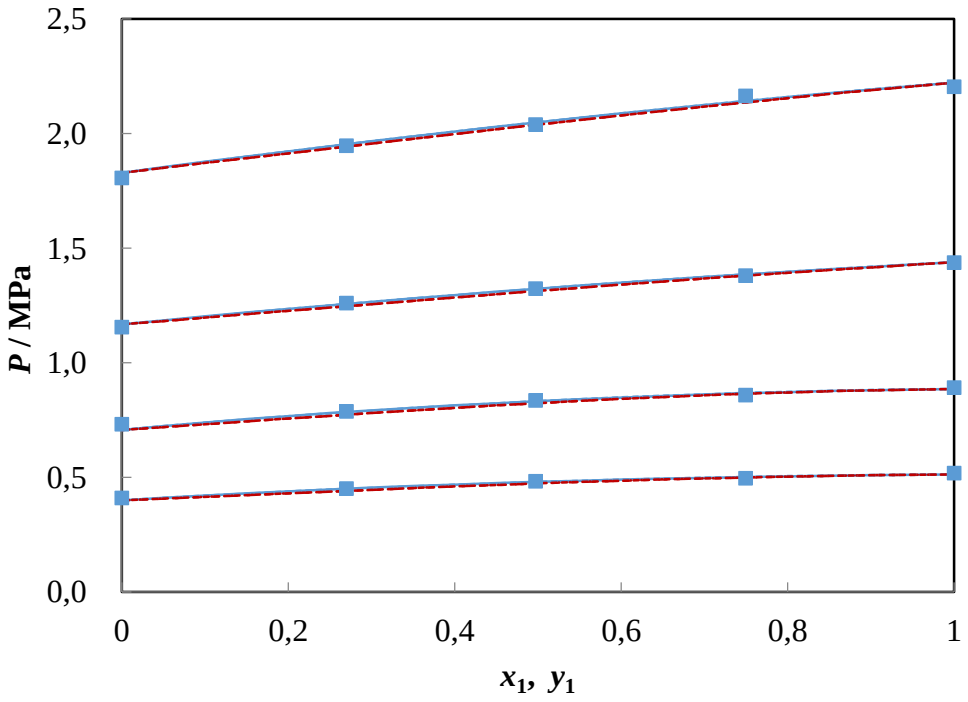

Figure 11. VLE for the R1243zf (1) + R245cb (2) binary system at four temperatures of 293.43, 313.41, 333.45, 353.52 K. (■): bubble point; dash lines: PR-MC-vdW model; solid lines: PR-MC-MHV2 model.

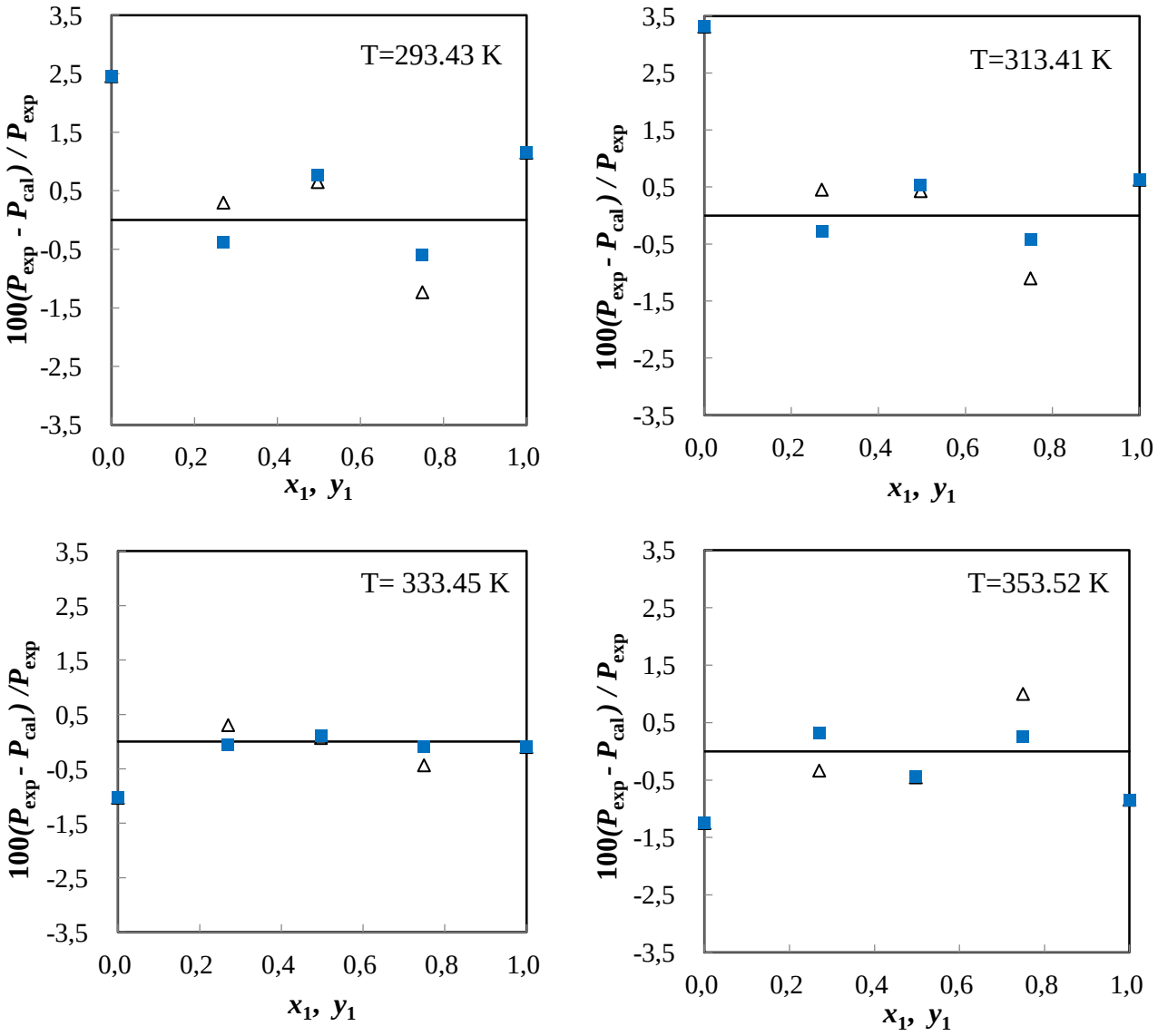

Figure 12. Relative deviation of pressure for the R1243zf (1) + R245cb (2) binary system from PR-MC-vdW and PR-MC-MHV2 model. (△): PR-MC-vdW model; (■): PR-MC-MHV2 model.

5. Conclusion

A novel method for determining critical point of pure compound or mixture is presented and tested. The method is based on determination of vapor and liquid densities at the vicinity of the critical point by visual method (observation of disappearance of the vapor-liquid interface). Critical properties of two binary systems of R1243zf + R1234yf and R1243zf + R245cb are investigated based on the new method. The critical point temperature, pressure, and density are determined via modeling vapor-liquid coexistence points to the combined equations of the scaling law and rectilinear diameters law. The critical properties are correlated by the Redlich-Kister type equation as a function of the composition. The results show non-linear relationship with mole fraction x_1 for the R1243zf + R1234yf binary system.

The bubble pressures of two binary systems are measured based on the static-synthetic method. The bubble pressures of R1243zf + R1234yf and R1243zf +R245cb are correlated by two cubic EoS (PR-MC-vdW and PR-MC-MHV2) and the corresponding phase diagrams are predicted. Both of two binary systems exhibit near-azeotropic behavior. Based on the deviation analysis, it is found that the PR-MC-MHV2 model exhibits better capabilities on VLE prediction.

Isothermal and isobaric VLE of the two binary systems are predicted at temperatures up to mixture critical point temperatures by PR-MC-MHV2 EoS. Good agreement is obtained between experimental critical point and predictions from the PR-MC-MHV2 EoS.

Acknowledgment

The authors gratefully acknowledge financial support from the China Scholarship Council for Z. Yang's Visiting (No. 201905290003).

References

Akasaka, R., 2016. Recent trends in the development of Helmholtz energy equations of state and their application to 3,3,3-trifluoroprop-1-ene (R-1243zf). Sci. Technol. Built Environ. https://doi.org/10.1080/23744731.2016.1208000

Akasaka, R., Tanaka, K., Higashi, Y., 2013. Measurements of saturated densities and critical parameters for the binary mixture of 2,3,3,3-tetrafluoropropene (R-1234yf) + difluoromethane (R-32). Int. J. Refrig. 36, 1341–1346. https://doi.org/10.1016/j.ijrefrig.2013.02.005

Bobbo, S., Nicola, G. Di, Zilio, C., Brown, J.S., Fedele, L., 2018. Low GWP halocarbon refrigerants: A review of thermophysical properties. Int. J. Refrig. 90, 181–201. https://doi.org/10.1016/j.ijrefrig.2018.03.027

Brown, J.S., Di Nicola, G., Fedele, L., Bobbo, S., Zilio, C., 2013. Saturated pressure measurements of 3,3,3-trifluoroprop-1-ene (R1243zf) for reduced temperatures ranging from 0.62 to 0.98. Fluid Phase Equilib. 351, 48–52. https://doi.org/10.1016/j.fluid.2012.09.036

Brown, J.S., Zilio, C., Brignoli, R., Cavallini, A., 2014. Thermophysical properties and heat transfer and pressure drop performance potentials of hydrofluoro-olefins, hydrochlorofluoro-olefins, and their blends. HVAC R Res. 20, 203–220. https://doi.org/10.1080/10789669.2013.854146

Coquelet, C., Chareton, A., Richon, D., 2004. Vapour-liquid equilibrium measurements and correlation of the difluoromethane (R32) + propane (R290) + 1,1,1,2,3,3,3-heptafluoropropane (R227ea) ternary mixture at temperatures from 269.85 to 328.35 K. Fluid Phase Equilib. 218, 209–214. https://doi.org/10.1016/j.fluid.2003.12.009

Coquelet, C., Ramjugernath, D., Madani, H., Valtz, A., Naidoo, P., Meniai, A.H., 2010. Experimental measurement of vapor pressures and densities of pure hexafluoropropylene. J. Chem. Eng. Data 55, 2093–2099. https://doi.org/10.1021/je900596d

Coquelet, C., Richon, D., 2009. Experimental determination of phase diagram and modeling: Application to refrigerant mixtures. Int. J. Refrig. https://doi.org/10.1016/j.ijrefrig.2009.03.013

Coquelet, C., Valtz, A., Théveneau, P., 2019. Experimental Determination of Thermophysical Properties of Working Fluids for ORC Applications. ORC Waste Heat Recover. Appl. 32, 137–144.

Dahl, S., Michelsen, M.L., 1990. High‐pressure vapor‐liquid equilibrium with a UNIFAC‐based equation of state. AIChE J. 36, 1829–1836. https://doi.org/10.1002/aic.690361207

Daubert, T.E., Hutchison, G., 1990. Vapor pressure of 18 pure industrial chemicals, in: AIChE Symposium Series. pp. 93–114.

Defibaugh, D.R., Moldover, M.R., 1997. Compressed and saturated liquid densities for 18 halogenated organic compounds. J. Chem. Eng. Data 42, 160–168. https://doi.org/10.1021/je960266e

Di Nicola, G., Brown, J.S., Fedele, L., Securo, M., Bobbo, S., Zilio, C., 2013. Subcooled liquid density measurements and PvT measurements in the vapor phase for 3,3,3-trifluoroprop-1-ene (R1243zf). Int. J. Refrig. 36, 2209–2215.

European Parliament, The Council of the European Union, 2006. Directive 2006/42/EC of the European Parliament and of the Council of 17 May 2006 on machinery, and amending Directive 95/16/EC (recast). Off. J. Eur. Union.

Gil, L., Otín, S.F., Embid, J.M., Gallardo, M.A., Blanco, S., Artal, M., Velasco, I., 2008. Experimental setup to measure critical properties of pure and binary mixtures and their densities at different pressures and temperatures. Determination of the precision and uncertainty in the results. J. Supercrit. Fluids 44, 123–138. https://doi.org/10.1016/j.supflu.2007.11.003

González, S., Jiménez, E., Ballesteros, B., Martínez, E., Albaladejo, J., 2015. Hydroxyl radical reaction rate coefficients as a function of temperature and IR absorption cross sections for CF3CH=CH2 (HFO-1243zf), potential replacement of CF3CH2F (HFC-134a). Environ. Sci. Pollut. Res. https://doi.org/10.1007/s11356-014-3426-2

Higashi, Y., Hayasaka, S., Shirai, C., Akasaka, R., 2015. Measurements of PρT properties, vapor pressures, saturated densities, and critical parameters for R 1234ze(Z) and R 245fa. Int. J. Refrig. 52, 100–108. https://doi.org/10.1016/j.ijrefrig.2014.12.007

Higashi, Y., Sakoda, N., 2018. Measurements of PvT Properties, Saturated Densities, and Critical Parameters for 3,3,3-Trifluoropropene (HFO1243zf). J. Chem. Eng. Data 63, 3818–3822. https://doi.org/10.1021/acs.jced.8b00452

Jia, X., Yang, J., Wu, J., 2020. Compressed liquid densities of binary mixtures of

difluoromethane (R32) and 2,3,3,3-tetrafluoroprop-1-Ene (R1234yf) at temperatures from (283 to 363) K and pressures up to 100 MPa. J. Chem. Thermodyn. 141, 105935. https://doi.org/10.1016/j.jct.2019.105935

Juntarachat, N., Beltran Moreno, P.D., Bello, S., Privat, R., Jaubert, J.N., 2012. Validation of a new apparatus using the dynamic and static methods for determining the critical properties of pure components and mixtures. J. Supercrit. Fluids 68, 25–30. https://doi.org/10.1016/j.supflu.2012.04.004

Kou, L., Yang, Z., Tang, X., Zhang, W., Lu, J., 2019. Experimental measurements and correlation of isothermal vapor-liquid equilibria for HFC-32 + HFO-1234ze (E) and HFC-134a + HFO-1234ze (E) binary systems. J. Chem. Thermodyn. 139, 105798. https://doi.org/10.1016/j.jct.2019.04.020

Lai, N.A., 2014. Thermodynamic properties of HFO-1243zf and their application in study on a refrigeration cycle. Appl. Therm. Eng. https://doi.org/10.1016/j.applthermaleng.2014.04.042

Lemmon, E.W., Bell, I.H., Huber, M.L., McLinden, M.O., 2018. NIST Reference Fluid Thermodynamic and Transport Properties Database (REFPROP), Version 10.0; Standard Reference Data; National Institute of Standards and Technology: Gaithersburg, MD. NIST Stand. Ref. Databasev23.

Lemmon, E.W., Bell, I.H., Huber, M.L., McLinden, M.O., 2013. NIST Standard Reference Database 23: Reference Fluid Thermodynamic and Transport Properties-REFPROP, Version 9.1, National Institute of Standards and Technology 135. https://doi.org/http://dx.doi.org/10.18434/T4JS3C

Mathias, P.M., Copeman, T.W., 1983. Extension of the Peng-Robinson equation of state to complex mixtures: Evaluation of the various forms of the local composition concept. Fluid Phase Equilib. https://doi.org/10.1016/0378-3812(83)80084-3

McLinden, M.O., Brown, J.S., Brignoli, R., Kazakov, A.F., Domanski, P.A., 2017. Limited options for low-global-warming-potential refrigerants. Nat. Commun. 8, 1–9. https://doi.org/10.1038/ncomms14476

Mclinden, M.O., Seeton, C.J., Pearson, A., 2020. New refrigerants and system configurations for vapor-compression refrigeration 1–7.

Meekel-lesavre, M., Richon, D., Renon, H., 1981. New Variable Volume Cell for Determining Vapor-Liquid Equilibria and Saturated Liquid Molar Volumes by the Static Method C, 284–289. https://doi.org/10.1021/i100003a017

Meskel-Lesavre, M., Richon, D., Renon, H., 1982. Bubble Pressures and Liquid Molar Volumes of the System Chlorotrifluoromethane-1,1,2-Trichlorotrifluoroethane. J. Chem. Eng. Data 27, 160–165. https://doi.org/10.1021/je00028a019

P. H. van Konynenburg, R. L. Scott, 1980. Critical lines and phase equilibria in binary van der Waals mixtures. Philos. Trans. R. Soc. London. Ser. A, Math. Phys. Sci. 298, 495–540. https://doi.org/10.1098/rsta.1980.0266

Peng, D.Y., Robinson, D.B., 1976. A New Two-Constant Equation of State. Ind. Eng. Chem. Fundam. https://doi.org/10.1021/i160057a011

Raabe, G., 2013. Molecular simulation studies on the thermophysical properties of the refrigerant blend R-445A. J. Chem. Eng. Data 58, 3470–3476. https://doi.org/10.1021/je400738r

Renon, H., Prausnitz, J.M., 1968. Local Compositions in Thermodynamic Excess Functions for Liquid Mixtures. AICHE J. 14, 135–143.

Rousseaux, P., Richon, D., Renon, H., 1983. A static method for determination of vapour-liquid equilibria and saturated liquid molar volumes at high pressures and temperatures using a new variable-volume cell. Fluid Phase Equilib. 11, 153–168. https://doi.org/10.1016/0378-3812(83)80055-7

Shank, R.L., 1967. Thermodynamic properties of 1,1,1,2,2-pentafluoropropane (refrigerant 245). J. Chem. Eng. Data 12, 474–480. https://doi.org/10.1021/je60035a004

Soo, C. B., Théveneau, P., Coquelet, C., Ramjugernath, D., Richon, D., 2010. Determination of critical properties of pure and multi-component mixtures using a “dynamic-synthetic” apparatus. J. Supercrit. Fluids 55, 545–553. https://doi.org/10.1016/j.supflu.2010.10.022

UNEP, 2016. The Kigali Amendment to the Montreal Protocol: HFC Phase-down. OzonAction Fact Sheet.

Valtz, A., El Abbadi, J., Coquelet, C., Houriez, C., 2019. Experimental measurements and modelling of vapour-liquid Mesures expérimentales et modélisation de l ’ équilibre vapeur-liquide du système. Int. J. Refrig. 107, 315–325.

https://doi.org/10.1016/j.ijrefrig.2019.07.024

Valtz, A., Laugier, S., Richon, D., 1986. Bubble pressures and saturated liquid molar volumes of difluoromonochloromethane-fluorochloroethane binary mixtures: experimental data and modelling. Int. J. Refrig. 9, 282–289. https://doi.org/10.1016/0140-7007(86)90123-4

Weber, L.A., Defibaugh, D.E., 1996. Vapor Pressure of 1 , 1 , 1 , 2 , 2-Pentafluoropropane. J. Chem. Eng. Data 9568, 762–764. https://doi.org/10.1021/je950312v

Yang, T., Siepmann, J.I., Wu, J., 2021. Phase Equilibria of Difluoromethane (R32), 1,1,1,2-Tetrafluoroethane (R134a), and trans-1,3,3,3-Tetrafluoro-1-propene (R1234ze(E)) Probed by Experimental Measurements and Monte Carlo Simulations. Ind. Eng. Chem. Res. 60, 739–752. https://doi.org/10.1021/acs.iecr.0c05442

Yang, Z., Tang, X., Wu, J., Lu, J., 2019. Experimental measurements of saturated vapor pressure and isothermal vapor-liquid equilibria for 1,1,1,2-Tetrafluoroethane (HFC-134a) + 3,3,3-trifluoropropene (HFO-1243zf) binary system. Fluid Phase Equilib. 498, 86–93. https://doi.org/10.1016/j.fluid.2019.06.020

Yang, Z., Valtz, A., Coquelet, C., Wu, J., Lu, J., 2020. Experimental measurement and modelling of vapor-liquid equilibrium for 3,3,3- Trifluoropropene (R1243zf) and trans-1,3,3,3-Tetrafluoropropene (R1234ze(E)) binary system. Int. J. Refrig. 120, 137–149. https://doi.org/10.1016/j.ijrefrig.2020.08.016